



An improved perspective in the representation of soil moisture: potential added value of SMOS disaggregated 1 km resolution product

Samiro Khodayar¹, Amparo Coll², Ernesto Lopez-Baeza²

¹ Institute of Meteorology and Climate Research (IMK-TRO), Karlsruhe Institute of Technology (KIT), Karlsruhe, Germany

² University of Valencia, Spain. Earth Physics and Thermodynamics Department. Climatology from Satellites Group

* Corresponding author. E-mail address: samiro.khodayar@kit.edu (S. Khodayar)

Institute for Meteorology and Climate Research, Karlsruhe Institute of Technology (KIT),

Postfach 3640, 76021 Karlsruhe, Germany



1 **Abstract**

2 This study uses the synergy of multiresolution soil moisture (SM) satellite estimates from the
3 Soil Moisture Ocean Salinity (SMOS) mission, a dense network of ground-based SM
4 measurements, and a Soil Vegetation Atmosphere Transfer (SVAT) model, SURFEX
5 (Externalized Surface) – module ISBA (Interactions between Soil-Biosphere-Atmosphere), to
6 examine, i) the comparison and suitability of different operational SMOS SM products to
7 provide realistic information on the water content of the soil as well as the added value of the
8 newly released SMOS Level 4 3.0 “all weather” disaggregated ~ 1 km SM (SMOS_L4^{3.0}),
9 and ii) its potential impact for improving uncertainty associated to SM initialization in land
10 surface modelling. Three different data products from SMOS-L3 (~ 25 km), L2 (~15 km), and
11 disaggregated L4 3.0 (~1km) are investigated. In situ SM observations over the Valencia
12 Anchor Station (VAS; SMOS Calibration/Validation (Cal/Val) site in Europe) are used for
13 comparison. The SURFEX-ISBA model is used to simulate point-scale surface SM (SSM)
14 and, in combination with high-quality atmospheric information data, namely ECMWF and the
15 SAFRAN meteorological analysis system, to obtain a representative SSM mapping over the
16 VAS. The sensitivity to SSM initialization, particularly to realistic initialization with
17 SMOS_L4^{3.0} to simulate the spatial and temporal distribution of SSM is assessed. Results
18 demonstrate: (a) all SMOS products correctly capture the temporal patterns, but, the spatial
19 patterns are not accurately reproduced by the coarser resolutions probably in relation to the
20 contrast with point-scale in situ measurements. (b) The potential of SMOS-L4^{3.0} product is
21 pointed out to adequately characterize SM spatio-temporal variability reflecting patterns
22 consistent with intensive point scale SSM samples on a daily time scale. The restricted
23 temporal availability of this product dictated by the revisit period of the SMOS satellite
24 compromises the averaged SSM representation for longer periods than a day. (c) A seasonal



25 analysis points out improved consistency during December-January-February and September-
26 October-November in contrast to significantly worse correlations in March-April-May (in
27 relation to the growing vegetation) and June-July-August (in relation to low SSM values < 0.1
28 m^3/m^3 and low spatial variability). (d) Perturbation simulations with the SURFEX-ISBA
29 SVAT (Soil-Vegetation-Atmosphere Transfer) model demonstrate the impact of the initial
30 SSM scenarios on its temporal evolution. (e) The combined use of the SURFEX-ISBA SVAT
31 model with the SAFRAN system, initialized with SMOS-L4^{3.0} 1 km disaggregated data is
32 proven to be a suitable tool to produce regional SM maps with high accuracy which could be
33 used as initial conditions for model simulations, flood forecasting, crop monitoring and crop
34 development strategies, among others.

35 *Key Words: soil moisture, SMOS 1-km disaggregated product, SURFEX, Valencia Anchor*
36 *Station, realistic initialization, SAFRAN*

37

38

39

40

41

42

43

44

45

46



47 **1. Introduction**

48 Reliability of climate and hydrological models is constrained by associated uncertainties, such
49 as input parameters. Among them, soil moisture is a variable of pivotal importance
50 controlling the exchanges of water and energy at the surface/atmosphere interface (Entekhabi
51 et al., 1996). Thus, it is a highly relevant variable for climate, hydrology, meteorology and
52 related disciplines (e.g. Seneviratne et al. 2010).

53 Soil moisture is greatly variable spatially, temporally and across scales. The spatial
54 heterogeneity of soil, vegetation, topography, land cover, rainfall and evapotranspiration are
55 accounted responsible (Western et al., 2002; Bosh et al., 2007). An adequate representation of
56 the high spatio-temporal variability of soil moisture is needed to improve climate and
57 hydrological modelling (Koster et al., 2004; Seneviratne et al., 2006; Brocca et al., 2010). Its
58 impact has been seen on time scales from hours to years (e.g., ~ 20 km scale: Taylor and
59 Lebel, 1998; droughts: Schubert et al., 2004; decadal drying of the Sahel: Walker and
60 Rowntree, 1977; hot extremes: Seneviratne et al., 2006b; Hirschi et al., 2011; decadal
61 simulations: Khodayar et al., 2014). To obtain an appropriate representation of this variable,
62 especially at high-resolution, is not an easy task mainly because of its high variability.
63 Methods for the estimation of soil moisture can be divided in three main categories, (i)
64 measurement of soil moisture in the field, (ii) estimation via simulation models, and (iii)
65 measurement using remote sensing. In general, in situ measurements are far from global (e.g.,
66 Robock et al. 2000), and model simulations present important biases. Therefore, we have to
67 rely on space-borne sensors to provide such measurements, but until recent times no
68 dedicated, long-term, moisture space mission was attempted (Kerr, 2007).

69 Nowadays, by means of remote sensing technology surface soil moisture is available at global
70 scale (Wigneron et al., 2003). The best estimations result from microwave remote sensing at
71 low frequencies (Kerr, 2007; Jones et al., 2011). The SMOS (Soil Moisture and Ocean



72 Salinity; Kerr et al., 2001) mission is the first space-borne passive L-band microwave (1.4
73 GHz) radiometer measuring at low frequency soil moisture over continental surfaces as well
74 as ocean salinity (Kerr et al., 2001, 2010). SMOS delivers global surface soil moisture
75 measurements (~ 0-5 cm depth) at 0600 a.m. and 0600 p.m. LT (local time) in less than 3-
76 days revisit at a spatial resolution of ~ 44 km. The benchmark of the mission is to reach
77 accuracy better than $0.04 \text{ m}^3/\text{m}^3$ for the provided global maps of soil moisture (Kerr et al.,
78 2001).

79 SMOS data is not exempt of biases. Validating remote sensing-derived soil moisture products
80 is difficult, e.g. due to scale differences between the satellite footprints and the point
81 measurements on the ground (Cosh et al., 2004). However, in the last years a huge effort has
82 been made to validate the SMOS algorithm and its associated products. With this purpose, in
83 situ measurements across a range of climate regions were used assessing the reliability and
84 accuracy of these products using independent measurements (Delwart et al., 2008; Juglea et
85 al., 2010; Bircher et al., 2012; Dente et al., 2012; Gherboudj et al., 2012; Sánchez et al., 2012;
86 Wigneron et al., 2012). The strategy adapted by the European Space Agency (ESA) was to
87 develop specific land product validation activities over well-equipped monitoring sites. An
88 example for this is the Valencia Anchor Station (VAS; Lopez-Baeza et al., 2005a) in eastern
89 Spain, which was chosen as one of the two main test sites in Europe for the SMOS
90 Calibration/Validation (Cal/Val) activities. The validation sites were chosen to be slightly
91 larger than the actual pixel (3dB footprint), thus, VAS covers a $50 \times 50 \text{ km}^2$ area. Within this
92 area, a limited number of ground stations were installed relying on spatialized soil moisture
93 information using the SVAT (Soil Vegetation Atmospheric Transfer) SURFEX (Externalized
94 Surface) model. Worldwide validation results reveal a coefficient of determination (R^2) of
95 about 0.49 when comparing the ~5 cm in situ soil moisture averages and the SMOS soil
96 moisture level 2 (SMOS-L2 ~ 15 km). For example, validation results by Bircher et al. (2012)



97 in Western Denmark show R^2 of 0.49-0.67 (SMOS retrieved initial soil moisture) and 0.97
98 (SMOS retrieved initial temperature). Besides, a significant under-/over-representation of the
99 network data (biases of -0.092 - 0.057 m^3/m^3) is also found. Over the Maqu (China) and the
100 Twente (The Netherlands) regions, the validation analysis resulted in R^2 of 0.55 and 0.51,
101 respectively, for the ascending pass observations, and of 0.24 and 0.41, for the descending
102 pass observations. Furthermore, Dente et al. (2012) pointed out a systematic SMOS soil
103 moisture (ascending pass observations) dry bias of about 0.13 m^3/m^3 for the Maqu region and
104 0.17 m^3/m^3 for the Twente region. Validation of the SMOS level 3 product (SMOS-L3 ~ 35
105 km) shows that the general dry bias in SMOS-L2 is also present in SMOS-L3 SM. This bias
106 is markedly present in the ascending products and shorter time series as described in Sanchez
107 et al. (2012) and Gonzalez-Zamora et al. (2015). In this case, the presence of dense vegetation
108 is seen to increase RMSE scores, whereas in low vegetated areas a lower dry bias is found
109 (Louvet et al. 2015).

110 Since the launch of the SMOS satellite, the processing prototypes of the SMOS L2 soil
111 moisture have evolved, and their quality has improved. Furthermore, efforts have been made
112 to cover the need of a reliable product with finer resolution for hydrological and climatic
113 studies where the spatial variability of soil moisture plays a crucial role, e.g. in the estimation
114 of land surface fluxes (evapotranspiration (ET) and runoff). Piles et al. (2011) presented a
115 downscaling approach to optimally combine SMOS' soil moisture estimates with MODIS
116 visible/infrared (VIS/IR) satellite data into 1 km soil moisture maps over the Iberian
117 Peninsula (IP) without significant degradation of the root mean square error (RMSE). This
118 product has been evaluated using the REMEDHUS (REd de MEDicion de la HUmedad del
119 Suelo) soil moisture network in the semi-arid area of the Duero basin, Zamora, Spain (Piles et
120 al. 2014). Results show that downscaling maintains temporal correlation and root mean
121 squared differences with ground-based measurements, hence, capturing the soil moisture



122 dynamics. A big limitation for this downscaling approach is the lack of information in cloudy
123 conditions, which significantly limits the availability and usefulness of this product. Trying to
124 tackle this problem, a new product, SMOS Level 4 3.0 “all weather” disaggregated ~ 1 km
125 SM (SMOS_L4^{3.0}, the previous product is hereafter named SMOS_L4^{2.0}) was developed, in
126 which the limitation on clouds is taken into account and has been recently made available by
127 SMOS-BEC (Barcelona Expertise Centre).

128 Up to now, SMOS-L3 and -L2 products have extensively been validated as described above
129 and used for assimilation purposes in models (e.g. De Lannoy et al. 2016; Leroux et al. 2016);
130 however, few studies deal with the disaggregated 1 km SMOS-L4^{0.2} and SMOS-L4^{0.3} products
131 (mostly in relation to wildfire activity). In this study, the synergy of satellite reprocessed
132 SMOS soil moisture data obtained with improved processors, model simulations with the
133 SVAT SURFEX-ISBA and in situ stations from the VAS soil moisture network are used for
134 evaluation of the soil moisture fields. The first objective of this paper is to provide
135 information about the advantages and drawbacks of the different data sets and to assess the
136 added value of the SMOS-L4^{3.0} product with respect to coarser resolution products. The
137 second objective is devoted to apply a methodology to derive soil moisture maps over the
138 VAS area to evaluate the usefulness of the SMOS-L4^{3.0} product regarding future applications
139 such as realistic initialization in model simulations to reduce associated uncertainty. The
140 proposed investigation covers a one year period (a complete hydrological cycle) and focuses
141 on the semi-arid VAS area and the IP where water availability and fire risk are big
142 environmental issues, thus, knowledge of soil moisture conditions is of pivotal importance.
143 Furthermore, as spring time soil moisture anomalies over the IP are believed to be a pre-
144 cursor to droughts and heat waves in Europa (Vautard et al. 2007; Zampieri et al. 2009),
145 accurate monitoring and prediction of surface states in this region may be key for
146 improvements in seasonal forecasting systems.



147 The following objectives are then pursued: (a) Examination of soil moisture temporal and
148 spatial distribution with SMOS-derived soil moisture products over the investigation domain
149 using a multi-resolution approach: L3 (~ 25 km), L2 (~15 km), and L4^{3.0} (~ 1 km), (b)
150 Validation with the in situ soil moisture measurements' network (VAS) to estimate the
151 reliability of the SMOS SM products, (c) Evaluation of the usefulness at different resolutions
152 and the added value of the 1 km product, (d) Modelization of point-scale soil moisture with
153 SURFEX-ISBA and spatialization over the VAS area using ground measurements for
154 verification, (e) Evaluation of the impact of realistic SM initialization using SMOS-L4^{3.0} on
155 point-scale and regional model simulations over the VAS area. This investigation is structured
156 as follows, in Section 2, the study area and the data sets are presented including the ground
157 measurements, the SMOS data products, and the SURFEX-ISBA model and related
158 atmospheric forcings used. Section 3 summarizes the methodology applied. The results are
159 discussed in Section 4. Finally, conclusions are drawn in Section 5.

160

161 **2. Study area and data set**

162 2.1 Investigation domain and in situ measurements over the VAS

163 The main investigation areas in this study are the Iberian Peninsula and the Valencia Anchor
164 Station (VAS) site located in eastern Spain (39.69°-39.22° N, -1.7°-(-1.11°) W). The VAS site
165 covering approximately a 50x50 km² area was established in December 2001 by the
166 University of Valencia as a Calibration/Validation (Cal/Val) site for different low-resolution
167 Earth Observation data products (Bolle et al., 2006). The extension and homogeneity of the
168 area as well as the mostly flat conditions (slopes lower than 2%) make it an ideal reference
169 site. Nevertheless, the small variations in the area, 750 to 950 m, influence the climate of the
170 region, which oscillates between semiarid to dry-sub-humid. Most of the area is dedicated to



171 vineyards (65%), followed by trees, shrubs, forest and industrial and urban cover types.
172 Mostly bare soil conditions are observed beside the vineyard growing season (March/April to
173 September/October). Mean temperatures in the region are between 12°C and 14°C with
174 annual mean precipitation about 450 mm, with maximums in spring and autumn. Within the
175 VAS, a network consisting of eight ThetaProbe ML2x soil moisture stations was deployed by
176 the Climatology from Satellites Group from the Earth Physics and Thermodynamics
177 Department at the University of Valencia. The eight in situ stations are distributed over a
178 10x10 km² area (Figure 1), according to land use, soil type, and other environmental
179 conditions. Details about the characteristics of each station are summarized in Table 1. Soil
180 moisture measurements every 10 min, mostly from 2006, were carried out for the top first 5
181 cm. More details about the VAS characteristics and soil moisture measurements could be
182 found in Juglea et al. (2010). Precipitation measurements over the IP and the VAS are from
183 the AEMET (Agencia Estatal de Meteorología; Spanish Weather Service) network.
184 Measurements every 10 min are available.

185 2.2 The SMOS surface soil moisture products

186 ESA's derived SMOS Soil Moisture Level 2 (SMOS-L2) data product, ~ 15 km, contains the
187 retrieved soil moisture and optical thickness and complementary parameters such as
188 atmospheric water vapour content, radio frequency interferences and other flags. The SMOS-
189 L2 algorithms have been refined since the launch of SMOS, resulting in more precise SM
190 retrievals (ARRAY, 2014). The Level 3 SM product, SMOS-L3, was obtained from the
191 operational CATDS archive. This is a daily product that contains filtered data. The best
192 estimation of SM is selected for each node when several multi-orbit retrievals are available
193 for a given day. A detection of particular events is also performed in order to flag the data.
194 The processing of the data separates morning and afternoon orbits. The aggregated products
195 are generated from this fundamental product. The Level 4 SM, SMOS-L4 2.0 data (SMOS-



196 L4^{2.0}), with 1 km spatial resolution is provided by BEC and covers the IP, Balearic Islands,
197 Portugal, South of France, and North of Morocco (latitudes 34°– 45° N and longitudes 10° W
198 – 5° E). A downscaling method that combines highly accurate, but low-resolution SMOS
199 radiometric information with high-resolution, but low sensitivity, visible-to-infrared imagery
200 to SSM across spatial scales is used to derive the SMOS-L4^{2.0} data (Piles et al 2010). The
201 impact of using different vegetation indices from MODIS with higher spatial and temporal
202 resolution in the downscaling method was explored in Sanchez-Ruiz et al. (2014), showing
203 that the use of more frequent and higher spatial-resolution vegetation information lead to
204 improved SM estimates. The latest SMOS-L4 product is the version 3.0 or “all weather”
205 (SMOS-L4^{3.0}), which is the product used and examined in this study. The downscaling
206 approach is based on Piles et al. (2014) and Sanchez-Ruiz et al. (2014), with the novelty of
207 introducing ERA-Interim Land Surface Temperature (LST) data in the MODIS LST/NDVI
208 scape. The evaluation of the SMOS-L4 2.0 and 3.0 products support the use of the “all
209 weather” version, since it does not depend on cloud cover and the accuracy of the estimates
210 with respect to in-situ data is improved or preserved (Piles et al. 2015 (Quality report)).

211 In this study, the SMOS-L2 V5.51 data coming from a L1C input product (obtained from
212 MIRAS measurements), the SMOS-L3 V2.72 and the SMOS-L4 V3.0 are employed.

213 2.3 The SURFEX-ISBA SVAT model

214 The SVAT model SURFEX (Externalized Surface, Le Moigne et al. 2009) – module ISBA
215 (Interactions between Soil-Biosphere-Atmosphere, Noilhan and Planton 1989) is used to
216 generate point-scale and spatially distributed SM spatial and temporal fields from initial
217 conditions and atmospheric forcing. SURFEX-ISBA was developed at the National Center for
218 Meteorological Research (CNRM), at Météo France, and it has been widely validated over
219 vegetated and bare surfaces (e.g. Calvet et al. 1998). The ISBA scheme uses the Clapp and
220 Hornberger (1978) soil water model and Darcy’s law for the estimation of the diffusion of



221 water in the soil, and allows 12 land use and related vegetation parameterization types. Crops
222 are considered for the VAS area since mainly vineyards, almond and olive trees and shrubs
223 compose the region.

224 The surface characteristics are considered in the SVAT input, roughness and the fraction of
225 vegetation are adopted from ECOCLIMAP (Masson et al. 2003), topography is obtained from
226 GTOPO (GTOPO30 Documentation) and soil types are defined using FAO (FAO, 2014).

227 To obtain an accurate simulation of soil moisture in the study area, the model was originally
228 calibrated by Juglea et al. (2010) to be applied over the entire site for any season/year.
229 Particularly relevant for this study is the specific definition of the soil hydraulic parameters
230 which they made for the VAS area, since most of the hydrological parameters are site
231 dependent. A new set of empirical equations as a function of the percentages of sand and clay
232 was defined using Cosby et al. (1984) and Boone et al. (1999). New definitions and
233 recommendations by Juglea et al. (2010) for the VAS area were adopted in this investigation.

234 *Atmospheric forcing information: ECMWF and SAFRAN*

235 High quality atmospheric forcing is needed to carry out accurate simulations. To run the
236 ISBA model, the following atmospheric forcing data are needed: air temperature and
237 humidity at screen level, atmospheric pressure, precipitation, wind speed and direction and
238 solar and atmospheric radiation. Three different sets of atmospheric forcing information are
239 used in this study; (a) meteorological data from 3 fully equipped stations in the OBS area,
240 MELBEX-I, MELBEX-II and VAS, (b) ECMWF (European Centre for Medium-Range
241 Weather Forecast) data, and (c) information from the SAFRAN (Système d'Analyse
242 Fournissant des Renseignements Atmosphériques à la Neige) meteorological analysis system
243 (Durand et al. 1999; Quintana-Seguí et al. 2008; Vidal et al. 2010).



244 Precipitation, air temperature, surface pressure, air specific humidity, wind speed and
245 direction, downward longwave radiation, diffuse shortwave radiation, downward direct
246 shortwave radiation, snowfall rate and CO₂ concentration are used as input data from the
247 meteorological stations aforementioned in the OBS area. A temporal resolution of 10 min is
248 available. From ECMWF, dew point and temperature at 2 m, pressure, precipitation and wind
249 components, are used as forcing data, with a 6 h temporal resolution and 0.125°x0.125°
250 spatial resolution. Precipitation, air temperature, surface pressure, air specific humidity, wind
251 speed and downward shortwave and longwave radiation from SAFRAN are used as input
252 information with a spatial resolution of 8x8 km² and an hourly temporal resolution. In this last
253 case, we have an optimal spatial and temporal distribution of the atmospheric forcing over the
254 VAS area (~ 50x50 km²) and a rare to find complete database to force the land surface model.
255 More details about the SAFRAN system and its validation in north-eastern Spain could be
256 found in Quintana-Seguí et al. (2016).

257

258 **3. Analysis methodology**

259 In order to investigate the characteristics and potential added values of fine-scale SMOS-
260 derived soil moisture, the spatial variability, the temporal evolution as well as the probability
261 distribution is investigated. With this purpose, SMOS-derived soil moisture products at
262 different spatial resolutions, in situ measurements and model simulations are jointly
263 evaluated.

264 The spatial distribution and temporal evolution of precipitation and SMOS-derived soil
265 moisture over the IP and the VAS area are assessed for the time period from December 2011
266 to December 2012 considering also hydrological seasons (DJF: December-January-February,
267 MAM: March-April-May, JJA: June-July-August, SON: September-October-November).



268 During 2012, the Hydrological Cycle in the Mediterranean Experiment (HyMeX; Dobrinski et
269 al. 2014) took place in the Western Mediterranean with the IP and particularly the Valencia
270 area as target areas. During the SON period of 2012, the Special Observation Period (SOP1;
271 Ducrocq et al. 2014) with intensive experimental deployment over the area took place. This
272 provides us with valuable information about the environmental conditions as well as the
273 occurrence of precipitation events in the investigation area. SMOS-L3 (~ 25 km), SMOS-L2
274 (~ 15 km), and SMOS-L4^{3.0} (~ 1km) are used for the evaluation of soil moisture distribution
275 at different grid spacing. Piles et al. (2014) pointed out that differences may exist between
276 SMOS-L3–L2 and the 1 km disaggregated soil moisture SMOS-L4 because of the distinct
277 methodology used to obtain these products. Only SMOS descending passes or a mean
278 between ascendant and descent passes are used to calculate mean daily values of SMOS-
279 derived soil moisture. Soil moisture derived from the afternoon orbits was found to be more
280 accurate than the morning passes (Piles et al. 2014). The fine temporal resolution of the model
281 simulations (1 h) and the observations (10 min) allow comparisons at the time of the SMOS
282 overpasses. Because of the 3-day revisit period of the SMOS swath, the IP will not be fully
283 covered by the satellite on daily basis. However, despite identified difficulties (radio
284 frequency interferences, missing data ...), the IP is well observed being 1.5 days the average
285 observations frequency over the IP. Only those images with coverage higher than 50% are
286 considered in our calculations. A conservative remapping to coarser resolutions is applied,
287 when required, to make comparisons among each other or with respect to ground-based
288 observations on equal terms. Remapping allows point to point comparisons between these
289 data sets. In addition to the yearly and seasonal approach, an exemplary short time period, 19
290 to 20 October of 2012, is considered. These correspond to the periods in which two extreme
291 precipitation events occurred, affecting south and eastern Spain (end of September; Khodayar
292 et al. (2015)) and the Ebro valley (at the end of October; Jansà et al. 2014), respectively.
293 Therefore, high variability in the soil moisture distribution is expected.



294 The coefficient of variation (CV), defined as the ratio of the standard deviation to the mean,
295 of the precipitation and soil moisture fields over the IP, the VAS (50x50 km²) and the OBS
296 (10x10 km²) area are examined for the analysis of the spatial variability of the
297 aforementioned fields. The soil moisture daily index ($SM_{index,i}$) is calculated to assess the
298 evolution pattern allowing the study of daily variations

299 $SM_{index,i} = (SM_{i+1} - SM_i) / SM_i$, where SM_{i+1} is the soil moisture of the day $i+1$ and SM_i is the
300 soil moisture of the day before i .

301 The reliability of SMOS-L2 and SMOS-L4^{3.0} soil moisture products is evaluated by
302 comparison with in situ soil moisture measurements in the OBS area. The spatial and
303 temporal variability are considered as well as the probability distribution. Different
304 approaches are applied: (a) the nearest grid point is selected for point-like comparisons
305 between SMOS-L2 and SMOS-L4^{3.0} against in situ soil moisture stations, to reduce sampling
306 biases in this region of diverse soil characteristics (Table 1), (b) SMOS-L4^{3.0} soil moisture
307 grid cells are averaged over the 10x10 km² area and compared to the mean from the soil
308 moisture network stations to address the issue related to spatial averaging. For the comparison
309 between the SMOS-L2 and the in situ observations: when single ground-based stations are
310 considered the closest SMOS pixel is selected, in case of considering the OBS (10x10 km²) or
311 VAS (50x50 km²) areas the mean over all pixels which centre falls within the area is used.
312 For the comparison with SMOS descending passes the corresponding values from in situ
313 measurements are considered. Additionally, a separation between wet days (precipitation over
314 1 mm/d) and dry days is applied to consider possible implications of wet/dry soils for SMOS
315 measurements.

316 Linear regression, the coefficient of determination (R^2), the mean bias (MB), and the root
317 mean square deviation (RMSD) are used to predefine the accuracy. A debiased or centred



318 RMSD (CRMSD) is applied to discriminate the systematic and random error components
319 removing the overall bias before calculating the RMSD.

320 Soil moisture modeling is performed by the use of the SVAT, SURFEX (Externalized
321 Surface) – module ISBA (Interactions between Soil-Biosphere-Atmosphere) from Météo-
322 France. Configuration and specifications described in Juglea et al. (2010), which proved
323 successful in adequately simulate the associated soil moisture heterogeneity over the wide
324 VAS surface (50x50 km²), are adapted in this study. Simulations start on 1 December 2011 at
325 00UTC and cover the whole investigation period until 31 December 2012 with an hourly-
326 output time resolution. Point-scale SURFEX-ISBA simulations over the soil moisture
327 network stations in the VAS domain are validated with the in situ measurements to assess the
328 usefulness of the model for further investigation, picturing the potential of the model in
329 simulating upper level soil moisture variability on different soil characteristics (Table 1). The
330 impact of different soil moisture initializations on the temporal evolution of upper-level soil
331 moisture is additionally evaluated using initialization perturbation simulations. Since
332 measurements in the area are available since 2003, a climatological mean is calculated for
333 each of the soil moisture stations and considered for initialization of the control simulations
334 (CTRL). Three additional initialization experiments are performed, a) with the daily mean of
335 the real observation (ground-based measurement) on the initialization day, b) the
336 climatological seasonal mean, c) the climatological monthly mean.

337 To try to simulate the spatial and temporal heterogeneity of the soil moisture fields over the
338 VAS surface, the SURFEX-ISBA scheme is used in combination with high quality forcing
339 data from ECMWF (hereafter SURFEX-ECMWF) and the SAFRAN system (hereafter
340 SURFEX-SAFRAN) for spatialization purposes. The benefit of initializing the simulations
341 with SMOS-L4^{3.0} data in comparison to climatological means is discussed. Two exemplary
342 initializations - in a wet period and a dry period are examined. A comparison between



343 SURFEX-SAFRAN point-scale and 10x10 km² mean simulations is done against ground
344 measurements to assess the accuracy of the simulated SSM maps.

345

346 **4. Results**

347 4.1 SMOS-derived soil moisture at different resolutions

348 4.1.1 Spatial variability on seasonal and sub-seasonal time scales

349 Atmospheric forcing, evapotranspiration (ET), soil texture, topographical features and
350 vegetation types have been recognized as relevant factors contributing to soil moisture
351 variability (Rosenbum et al. 2012). The response of soil moisture to precipitation changes
352 largely depends on soils water capacity and climatic zones. Particularly, in dry climates such
353 as the IP, soil moisture quickly reacts to changes in precipitation (Li and Rodell 2013).
354 Precipitation variability and mean are positively correlated, thus, an increase in precipitation
355 yields wetter soils, which in turn results in higher spatial variability of soil moisture.

356 In the autumn period, the western Mediterranean is characterized by a large thermal gradient
357 between the atmosphere and the sea (Duffourg and Ducrocq, 2011, 2013) resulting in intense
358 precipitation extremes (Raveh-Rubin and Wernli 2015). Precipitation in the IP during the
359 autumn (SON) period of 2012 was above average (Khodayar et al. 2015). It is also the
360 hydrological season in which higher variability in the soil moisture is observed as a result of
361 the precipitation distribution (period used hereafter for investigation). The positive anomaly is
362 largely caused by two unique events, i.e. at the end of September (27-29) affecting south and
363 eastern Spain and at the end of October (19-20) affecting the Ebro valley (Jansà et al. 2014).

364 Figure 2a shows the north-south precipitation gradient for the SON period mean. The SSM
365 satisfactorily reflects this gradient (Figure 2b), but, more markedly for the SMOS-L3 and



366 SMOS-L2 than the higher resolution SMOS-L4^{3.0} showing lower standard deviation, SMOS-
367 L3($\sim 0.15 \pm 0.01$), SMOS-L2($\sim 0.17 \pm 0.01$), SMOS-L4($\sim 0.22 \pm 0.007$). The same performance is
368 seen over the VAS domain (not shown). The SSM variability associated to the extreme
369 precipitation events in this period is not well represented in the SMOS-L4^{3.0} seasonal mean.
370 Table 2 shows the number of days (percentage) in which there is more than 50 % of data over
371 the IP for each SMOS product. These periods have been used as basis for the calculation of
372 the spatial distributions in Figure 2b. SMOS-L3 (88 %) and SMOS-L2 (84 %) show a good
373 coverage and similar number of days. However, a large difference is observed with respect to
374 the SMOS-L4^{2.0} product with only 28 days (32 %) of adequate coverage for the period of
375 SON 2012. This is due to the problematic associated to the downscaling approach used to
376 obtain the 1 km soil moisture maps, in which the lack of Land Surface Temperature (LST)
377 information from MODIS visible/infrared (VIS/IR) satellite data in cloudy conditions (section
378 2.2) constrains derived-SSM information. The availability and usefulness of this product is
379 therefore significantly reduced. The new product L4^{3.0}, used in this study, in which the
380 previous limitation is resolved using ERA-Interim-derived LST information, shows a
381 coverage percentage in the order of 92 %, even higher than the SMOS-L3 and -L2 products.
382 However, Figure 2b demonstrates that the spatial representation of the seasonal mean does not
383 improve with this product, as a consequence of the limited temporal availability of the
384 SMOS-derived SSM product dictated by the revisit period of the satellite.

385 In Figure 3, only common available days from all different operational levels are selected for
386 an inter-SMOS product comparison. When remapped to the same resolution (coarser grid
387 spacing) comparable values are identified between SMOS-L3, -L2 and -L4^{3.0} for the JJA and
388 SON period, whereas relevant differences are pointed out from December to May. In this last
389 period, we identify higher means for the SMOS-L4^{3.0} product and SMOS-L3 with respect to



390 SMOS-L2, which is in agreement with a systematic dry bias identified for SMOS-L2 also in
391 previous studies (section 1).

392 At sub-seasonal scales, e.g. event scale on the 19-20 November 2012 (Figure 4), the SMOS-
393 L4^{3.0} product shows SSM mean and variability in the same range of the SMOS-L2 and -L3
394 products, but with a finer-improved resolution representation of the spatial distribution.
395 Comparisons with the mean ground-based SSM at the VAS (OBS area: 0.25 ± 0.0002) show
396 better agreement with the mean SSM from the SMOS-L4^{3.0}-1 km disaggregated product
397 (0.23 ± 0.002) and poorer correlation with SMOS-L2 (0.20 ± 0.002). The problematic of SMOS-
398 L4^{3.0} on seasonal time scales vanishes at sub-seasonal (event) scales where the potential
399 added value of the 1 km product is manifest.

400 4.1.2 Temporal evolution of surface soil moisture data sets

401 The SMOS and in situ measured SSM time series are investigated in this section. To assess
402 the behaviour and variability of these data sets we consider, (a) the *soil moisture daily index*,
403 to investigate the pattern of such evolution based on daily variations, and (b) the *coefficient of*
404 *variation (CV)*, for the analysis of the spatial variability and its evolution in time (Figure 5).
405 The temporal behavior of SSM averaged over the IP, the VAS domain, and the OBS area are
406 compared in Figure 6. SMOS afternoon (descendant; Piles et al. 2014) orbits are selected as
407 well as observations at the time of the SMOS overpasses. For the IP and VAS, SMOS-L2 and
408 SMOS-L4^{3.0} have been remapped to the coarser grid spacing for an adequate comparison.
409 Ground-based observations are aggregated using a mean over all stations for comparison with
410 the corresponding SMOS-L4^{3.0} data (the closest grid point is selected).

411 Overall, the averaged SMOS-L2 and -L4^{3.0} data over the IP are much more variable than the
412 SMOS-L3, showing a more extreme daily index (SMOS-L2: -1 to 2; SMOS-L4^{3.0}: -0.7 to
413 1.45). Over the VAS, SMOS-L2 is clearly more variable than the higher resolution SMOS-



414 L4^{3.0}. But, the last one shows a wider range of values as well as more extreme daily index
415 values when compared to the averaged in situ soil moisture measurements. The CVs of the
416 spatially averaged SMOS-L4^{3.0} is lower than those of SMOS-L3, -L2 and in situ observations
417 indicating that this data are less scattered. Despite detected differences within in situ
418 observations, SMOS responds well to soil moisture variations over time.

419 Although absolute values are not totally captured, all three SMOS products adequately
420 reproduce the temporal dynamics at a regional scale. The systematic dry bias present on
421 SMOS-L2 data (Piles et al. 2014) is evident particularly on the first half of the year. A mean
422 bias in the order of -0.09 to -0.07 m³/m³ is identified for the DJF-MAM period; this difference
423 is reduced to -0.02 m³/m³ for the JJA-SON period (Table 3). During the DJF-MAM period the
424 vineyards are bare, only the vine stocks are present. The water content of the vine stocks
425 negatively impacts the SMOS measurements (Schwank et al. 2012).

426 Good agreement is found between the SMOS-L4^{3.0} product and the mean of the in situ
427 observations (the network's variability (shaded grey) contains the SMOS-L4^{3.0} data). Scores
428 confirm this result particularly for the periods DJF and SON (slope~1, R²~0.7). Poorer
429 correlation is found for the MAM (slope~0.6, R²~0.4). In this period, soil moisture maxima
430 immediately after the precipitation events are not always well captured by the SMOS-L4^{3.0}
431 data, showing additionally a too rapid drying after this. This observation agrees with the
432 SMOS' inability of correctly measuring in situations when liquid water is present at the soil.
433 The measured signal is perturbed during the vegetation growing season, which could explain
434 the worse statistics. On the other hand, during JJA, low slope~0.1 and R²~0.01 could be in
435 relation to SSM values close to or lower than 0.1 m³/m³ and very low spatial variability,
436 which was found to be necessary for an adequate performance of the algorithm used for the
437 derivation of the SMOS-L4 1 km product in Molero et al. (2016).

438 4.2 Spatial comparison at high-resolution: SMOS-L4^{3.0} versus ground measurements



439 High-resolution spatio-temporal correlations are assessed by spatial comparison with in situ
440 observations. Characteristics of each of the in-situ stations are presented in Table 1. A
441 seasonal analysis is performed focusing on the selected year of measurements covering a
442 complete hydrological cycle (from 1 December 2011 to 31 December 2012). Comparisons
443 between SMOS-L2 and ground measurements are additionally included. In Figure 7, the
444 scatter plots display (a) possible differences between dry and wet days (> 1 mm/d), and (b, c)
445 the agreement between remotely sensed and in situ soil moisture measurements from the OBS
446 network using the seasonal classification. To consider any uncertainties arising from spatial
447 averaging, ground measurements are compared to point like and 10×10 km² SSM means. The
448 10×10 km² area used covers the OBS area, i.e., the network of in situ measurements within
449 the VAS. For comparison, all grid points from SMOS-L4^{3.0} and SMOS-L2 included within
450 the area are considered. Statistics for individual comparisons at all stations are summarized in
451 Table 3.

452 In Figure 7a, the separation between days with and without precipitation (< 1 mm/d) points
453 out similar correlations during dry than wet days (RMSD ~ 0.015 , $R^2 \sim 0.7$) for SMOS-L4^{3.0},
454 whereas a slightly better agreement is found for the dry days (not shown) for SMOS-L2. A
455 systematic mean dry bias of about 0.05 (dry days) to 0.08 (wet days) m³/m³ is assessed for
456 SMOS-L2, while a lower bias with changing sign is identified for the L4^{3.0} product (~ 0.005
457 (wet days); ~ -0.02 (dry days)). Comparisons using the corresponding mean over the 10×10
458 km² OBS area, in Figure 7b and Table 3, show good agreement with respect to the SMOS-
459 L4^{3.0} and poorer scores for SMOS-L2 (only one grid point of SMOS-L2 is located within the
460 OBS area). Worse consistency is found in both cases for the MAM and JJA periods. CRMSD
461 is in all cases in the required range of ≤ 0.04 m³/m³. Point-like comparisons with the
462 individual in situ stations, in Figure 7c and Table 3, show that spatial patterns are captured at
463 1km with RMSD ~ 0.007 to 0.1 m³/m³ but, in most cases, accuracy for SMOS-L4^{3.0}-1 km



464 disaggregated product is within the required range of less than $0.04 \text{ m}^3/\text{m}^3$ (not shown).
465 Higher RMSD is found for SMOS-L2, ~ 0.008 to $0.13 \text{ m}^3/\text{m}^3$, accounting for the previously
466 identified dry bias ($\sim (-0.14) - (-0.02)$) reduced in SMOS-L4^{3.0} ($\sim (-0.08) - (-0.01)$). The
467 CRMSD is in all cases $\leq 0.04 \text{ m}^3/\text{m}^3$. For all stations, better correlations are found in DJF and
468 SON and poorer scores in JJA and MAM, in agreement with the areal-mean comparisons
469 (section 4.1.3). Best scores are obtained for Nicolas, VAS and La Cubera stations, probably in
470 relation to their common soil type distribution, over vineyards, and homogeneous conditions,
471 over a plain (Figure 8a, Table 3). The SON time period reveals the best agreement, at this
472 time the vineyards are completely grown (however, senescent thus containing less water) and
473 SSM exhibits substantial spatial variability driven by precipitation and irrigation thus
474 improving spatio-temporal correlations. Worse statistics are found for Melbex-I, Melbex-II
475 and Ezpeleta, probably in relation to the location of the soil moisture probes in rockier and
476 orographically more complex areas, also in proximity to forestall and man-made construction
477 areas.

478 The soil moisture probability distribution function (PDF; Figure 8b) of all in situ
479 measurements versus SMOS-L4^{3.0} data reveals that the later overestimates SSM below 0.1
480 m^3/m^3 , values mainly observed during the JJA period. But, an underestimation occurs in the
481 range between 0.1 and $0.3 \text{ m}^3/\text{m}^3$, which is consistent with the identified underestimation of
482 maximum soil moisture reached after a precipitation event and the rapid drying of the soil in
483 comparison to the much slower response seen in the observations during the MAM period
484 (Figure 6c).

485 4.3 SURFEX model simulations and realistic initialization with 1-km soil moisture data

486 4.3.1 SURFEX model simulations of selected stations and realistic initialization



487 Land surface models are commonly used to analyse regional soil moisture estimates.
488 Initialization of land surface models is a crucial issue and its impact on the accuracy of model
489 estimation is widely recognized to be significant. When observations are not available, soil
490 moisture initialization is generally performed with simulated climatological mean values. In
491 this section, different sensitivity experiments with the SURFEX-ISBA SVAT model are
492 performed to investigate the impact of initialization in the simulation of the spatio-temporal
493 evolution of point-scale soil moisture and regional SSM fields.

494 As a first step, the performance of the SURFEX-ISBA SVAT model is evaluated. SURFEX-
495 ISBA point-like simulations are performed for all in situ soil moisture stations at the VAS
496 area to assess the usefulness of the model for further investigation (Table 4). To obtain an
497 accurate simulation of soil moisture in the area, the model has been calibrated and particular
498 characteristics have been considered following the recommendations by Juglea et al. (2010)
499 for each of the stations. The complete hydrological cycle (from 1 December 2011 to 31
500 December 2012) is simulated for each station.

501 SURFEX-ISBA simulations show good agreement with soil moisture ground-based
502 observations at all stations, adequately capturing the associated spatio-temporal variability
503 (slope~1, $R^2 \sim 0.7$ to 0.9 ; MB~ $0.1 \text{ m}^3/\text{m}^3$; CRMSD~ $0.02 \text{ m}^3/\text{m}^3$). It can be concluded that the
504 model performs well and is therefore suitable for further investigation. The seasonal analysis
505 points out the best simulations in the SON period ($R^2 \sim 0.9$ for all stations), but CRMSD is \leq
506 $0.04 \text{ m}^3/\text{m}^3$ for all stations at all periods.

507 Four experiments are performed modifying the initial soil moisture scenario using: (a) the
508 mean of the ground-based measurement on the day of the initialization (realistic initialization;
509 REAL-I), (b) the mean over the December month from the ground-based measurements
510 (MONTH_I), (c) the seasonal mean (DJF) from the ground-based measurements (SEASON-I)
511 and (d) the climatological ground measurements soil moisture mean over the last 10 years for



512 the December period (Figure 9a). Deviations of the sensitivity experiments with respect to the
513 mean of ground measurements reveal an impact during the whole simulation period even
514 though initial scenarios were close to each other. Even after strong precipitation events, which
515 reduce RMSD, the soil moisture evolution is affected by the initialization. REAL-I
516 simulations show the best agreement with in situ observations ($R^2 \sim 0.9$; CRMSD ~ 0.02
517 m^3/m^3). Thus, this realistic initial scenario based on in situ soil moisture observations is
518 hereafter used for model initialization in our control experiments. Temporal mean
519 comparisons for each station are presented in Figure 9b and Table 4 using the above described
520 REAL-I initialization scenario.

521 4.3.2 Spatialization

522 With the purpose of simulating soil moisture over a whole SMOS pixel, Juglea et al. (2010)
523 combined the SURFEX-ISBA model and ground and meteorological observations in the
524 study area. In this section, to obtain an accurate mapping of soil moisture over the VAS
525 ($50 \times 50 \text{ km}^2$) we discuss a different methodology for the spatialization of SURFEX-ISBA
526 simulations. Atmospheric forcing information both from ECMWF and SAFRAN is used as
527 input data (hereafter SURFEX-ECMWF and SURFEX-SAFRAN simulations, respectively).
528 SMOS-L4^{3.0}-1 km disaggregated values are used for initialization. In-situ soil moisture
529 observations over the VAS area are considered for verification. Soil moisture initialization in
530 spatialized SURFEX simulations requires a single representative value for the whole
531 simulation area. In this case, we use as input the SMOS-L4^{3.0}-1 km disaggregated soil
532 moisture mean over the whole simulation area for the initialization day. For comparison, the
533 mean of all ground-based observations is also used for the initialization.

534 As a first step, point-scale SURFEX-ECMWF and SURFEX-SAFRAN simulations covering
535 the whole investigation period are performed for all in situ soil moisture stations to examine
536 its ability to reproduce soil moisture dynamics. Ground measurements at each station are used



537 for initialization. Scores clearly indicate better agreement with all in situ observations for the
538 SURFEX-SAFRAN simulations (slopes \sim 1, $R^2\sim$ 0.9, RMSD $<$ 0.1 m³/m³), rather than the
539 SURFEX-ECMWF simulations (slopes $>$ 1, $R^2\sim$ 0.6, and RMSD $>$ 0.1 m³/m³).

540 In a second step, SURFEX-ECMWF and SURFEX-SAFRAN simulations are spatialized to
541 obtain maps of soil moisture over the investigation area. In our CTRL simulations, the daily
542 soil moisture from the mean of the in-situ measurements on the initialization day is used for
543 model initialization. Mean SSM from in situ measurements for the whole investigation period
544 is in the order of 0.14 ± 0.005 , whereas SURFEX-ECMWF derived SSM field is about
545 0.18 ± 0.007 and SURFEX-SAFRAN derived SSM field is 0.15 ± 0.002 , thus, closer to ground-
546 based observations. Performing a seasonal analysis, we demonstrate that this consistency is
547 maintained for all seasons (not shown). The higher resolution of the SAFRAN-atmospheric
548 forcing better reproduces the high spatial heterogeneity over the VAS area resulting in
549 improved mapping of simulated SSM.

550 Initialization of the SURFEX-SAFRAN combination using SMOS-L4^{3.0} is examined. Two
551 sensitivity simulations are performed using for the initial soil moisture scenario, (a) the daily
552 soil moisture mean from the SMOS-L4^{3.0} data (which is generally close to observations; EXP-
553 SMOS), and (b) the climatological soil moisture from observations (daily mean over 10 years,
554 which has been selected to be far from observations; EXP-CLIM). These experiments are
555 initialized in dry periods, following Khodayar et al. (2014) recommendations, to maximize
556 the impact, and run for about 3-4 months. In the first case, initialization is performed in a
557 winter month (December) and the whole simulation period remains almost dry. In the second
558 case, a summer month (July) is chosen for the initialization and it is followed by a wet autumn
559 period with frequent heavy precipitation events in the area.

560 The temporal evolution of the RMSD (Figure 10a) demonstrates that the initial soil moisture
561 scenario influences its evolution until the end of the simulation, in agreement with previous



562 results in section 4.3.1. Larger deviations occur during dry periods, in both scenarios. Longer
563 spin-up times, defined as the time that soil needs to reestablish quasi-equilibrium, characterize
564 the dry scenario. It is after heavy precipitation events that deviations decrease. Soil quickly
565 reacts to changes in the precipitation field in the semi-arid IP. When the upper level soil gets
566 close to saturation soil memory is almost lost. Before the high precipitation events, SSM
567 evolves following the direction of the initial perturbation, i.e., higher initial SSM yields
568 higher SSM, however, a stochastic behaviour is identified afterwards.

569 As an example, differences in the spatial distribution of soil moisture for the winter/dry period
570 simulation are discussed (Figure 10b). A relevant difference in the mean is identified when
571 compared to the CTRL simulation (0.17 ± 0.004): EXP-CLIM (0.014 ± 0.003), EXP_SMOS
572 (0.17 ± 0.003). Clearly, better agreement is found in this last case.

573 Considering the EXP-SMOS initialization scenario simulation, a comparison between
574 simulated point-like and the $10 \times 10 \text{ km}^2$ mean against corresponding ground measurements
575 was done for verification (Figure 10c). Correlations in the order of $R^2 \sim 0.9$ confirm that the
576 combined use of SURFEX-SAFRAN and SMOS-L4^{3.0} for initialization successfully
577 reproduces soil moisture spatial and temporal variability becoming an optimal tool for
578 mapping soil moisture heterogeneity over a study region for diverse purposes.

579

580 **5. Discussion and conclusions**

581 High-resolution soil moisture products are essential for our understanding of hydrological and
582 climatic processes as well as improvement of model skills. Due to its high spatial and
583 temporal variability, it is a complicated variable to assess. Mapping high-resolution soil
584 moisture fields using intensively collected in-situ measurements is infeasible. Thus, state of
585 the art high-resolution modelling and satellite-derived products have to fill this gap, although



586 verification is needed. In this study, we provide information about the advantages and
587 drawbacks of soil moisture SMOS satellite products at different operational levels examining
588 the potential of the state of the art SMOS-L4^{3.0}-1 km disaggregated product for assessment of
589 soil moisture variability, and improvement of SVAT simulations through realistic model
590 initialization. The proposed analysis focuses on the semi-arid IP and covers the one year
591 period of 2012 (from December 2011 to December 2012).

592 The SMOS-L4^{3.0}-1km product is compared to different resolution soil moisture data products
593 from SMOS, namely SMOS-L3 (~ 25 km) and SMOS-L2 (~15 km). Their ability in
594 reproducing soil moisture dynamics and heterogeneity and the added value of SMOS-L4 is
595 examined using a dense network of ground-based soil moisture measurements over the
596 Valencia Anchor Station (VAS; one of the SMOS test sites in Europe) for verification.
597 Perturbation simulations of point-scale surface soil moisture are investigated to assess the
598 sensitivity to soil moisture initialization. The Soil Vegetation Atmosphere Transfer (SVAT)
599 model SURFEX (Externalized Surface) – module ISBA (Interactions between Soil-
600 Biosphere-Atmosphere) is employed. Furthermore, the SURFEX-ISBA model is used in
601 combination with the ECMWF forcing information (SURFEX-ECMWF) and the SAFRAN
602 meteorological analysis system (SURFEX-SAFRAN) to obtain a representative soil moisture
603 representation over the VAS area. The sensitivity of the SURFEX-SAFRAN scheme to
604 simulate the heterogeneity of surface soil moisture applying realistic initialization with
605 SMOS_L4^{3.0} ~1 km product is investigated.

606 Correlation with precipitation is traceable in the temporal evolution of in situ ground
607 measurements and SMOS-derived soil moisture products. On seasonal time scales, SMOS-L3
608 (~ 25 km) and SMOS-L2 (~15 km) adequately represent the soil moisture gradient and high
609 soil moisture episodes in relation to the precipitation distribution. However, the seasonal
610 representation of SMOS-L4^{3.0}-1 km soil moisture does not capture these maxima despite the



611 novelty of introducing ERA-Interim LST data in the MODIS LST/NDVI space (Piles et al.
612 2014; Sanchez-Ruiz et al. 2014), probably due to the so different spatial resolution of ERA-
613 Interim and MODIS. This new downscaling approach greatly enhances the potential
614 applicability of the data for those days/periods in which measurements are available, but
615 cannot fill in those periods without measurements dictated by the revisit period of the SMOS
616 satellite, hence, compromising the soil moisture representation as a mean for longer periods
617 than a day. On sub-seasonal time scales, when SMOS images are available, the SMOS-L4^{3.0}
618 high-resolution product shows its potential. It adequately captures the surface soil moisture
619 variability in association with the precipitation field, also when extreme precipitation takes
620 place.

621 Characteristics of SMOS-L4^{3.0} soil moisture fields are closer to in-situ observations than
622 SMOS-L3 and -L2 products. Comparisons with in-situ measurements reveal that, generally,
623 all three SMOS products adequately reproduce the soil moisture temporal dynamics meeting
624 the desired accuracy of the mission (0.04 m³/m³); however, the spatial patterns did not reach
625 the expected precision in agreement with former studies in other regions (Gonzalez-Zamora et
626 al. 2015). The contrast between point-scale in-situ measurements and the coarse resolution of
627 the satellite observations is an issue that should be considered. A systematic dry bias,
628 particularly evident in the first half of the year (December to May), is identified in the SMOS-
629 L2 data, also observed in former investigations. The negative impact of the water content of
630 the vine stocks (vineyards are bare in this time period) on the SMOS measurements and the
631 coarser resolution result in poorer scores of the SMOS-L2 when compared to in-situ
632 observations. The SMOS-L4^{3.0} product and the mean of the in-situ observations show a good
633 agreement in general. This is consistent with the finer resolution of this product which better
634 captures local information on the 1 x 1 km pixel, whereas coarser products smooth out this
635 vital information.



636 The SMOS-L4^{3.0} soil moisture probability distribution function (PDF) in comparison to that
637 of the in-situ measurements reveals a SMOS overestimation below 0.1 m³/m³ and an
638 underestimation in the range between 0.1 to 0.3 m³/m³. A seasonal analysis points out better
639 scores for the DJF and SON periods, whereas poorer correlation is found for the MAM and
640 JJA periods. In the MAM period, an under-representation of the rainy events is found, as well
641 as faster and stronger drying changes coinciding with the vegetation growth season. In JJA,
642 the very low soil moisture values (< 0.1 m³/m³) with associated low spatial variability results
643 in low R². During dry and wet days (> 0.1 mm/d), similar correlations are found for SMOS-
644 L4^{3.0} comparisons with in-situ observations. A low bias with changing sign is identified for
645 the L4^{3.0} product (~ 0.005 (wet days); ~ -0.02 (dry days)). SMOS-L2 reveals slightly better
646 agreement for the dry days and a systematic mean dry bias of about 0.05 (dry days) to 0.08
647 (wet days) m³/m³.

648 Point-like and 10x10 km² comparisons show good agreement with respect to the SMOS-L4^{3.0}
649 and poorer scores for SMOS-L2 (e.g. DJF period: SMOS-L3/-L2: Slope:1.1/1.0, R²:0.5/0.7,
650 Bias:-0.09/(-0.03)). CRMSD is in the required range of ≤ 0.04 m³/m³ in most cases.
651 Comparison of the SMOS-L4^{3.0} data with ground soil moisture measurements from the eight
652 stations in the network (10x10 km²) over the VAS area shows that the spatial patterns are
653 captured at 1 km with RMSD~ 0.007 to 0.1 m³/m³ (5 out of the 6 stations investigated show
654 an accuracy of less than 0.04 m³/m³, benchmark of the SMOS mission). The best correlations
655 are in DJF and SON, and poorer scores in MAM and JJA, in agreement with the areal-mean
656 comparisons. SMOS-L4^{3.0} data shows better agreement at those stations over plain areas and
657 with uniform conditions (vineyards), against those over more complex and less homogeneous
658 terrains (rocky soils and areas close to forestall and man-made constructions).

659 The impact of initialization scenarios on the simulation of SSM is investigated by means of
660 SURFEX-ISBA SVAT simulations. Firstly, the performance of the land surface model is



661 evaluated. Simulations covering the whole investigation period over all in-situ measurement
662 stations at the VAS area have been carried out. In all cases, simulations show good agreement
663 with ground-based observations. Mean values are well reproduced for all stations and the
664 temporal variability is well captured ($R^2 \sim 0.7$ to 0.95 ; $RMSD \sim 0.02$). Four sensitivity
665 experiments using different initial scenarios are performed, (a) the mean of the ground-based
666 measurement on the day of the initialization (realistic initialization; REAL-I), (b) the mean
667 over the December month from the ground-based measurements (MONTH_I), (c) the
668 seasonal mean (DJF) from the ground-based measurements (SEASON-I) and (d) the
669 climatological soil moisture mean over the last 10 years for the December period. Deviations
670 larger than zero are present during the whole simulation period demonstrating the impact of
671 the initial soil moisture scenarios on its temporal evolution, even when close initial conditions
672 are considered. As expected, the use of real observations on the initialization day shows the
673 best agreement ($R^2 \sim 0.9$; $CRMSD \sim 0.02 \text{ m}^3/\text{m}^3$).

674 In a further step, SURFEX-ISBA simulations are combined with ECMWF and SAFRAN
675 atmospheric forcing information to obtain soil moisture maps over the VAS domain. The
676 higher resolution of the SAFRAN forcing data as well as the larger number of input variables
677 result in higher correlations with in-situ SSM measurements, hence, offering a good base for
678 investigating the potential impact of the soil initialization with SMOS-L4^{3.0}-1 km
679 disaggregated soil moisture.

680 The sensitivity of SURFEX-SAFRAN SSM field simulations to an initialization with realistic
681 SSM values from the SMOS-L4^{3.0} data set is compared to that using daily climatological
682 means. The model is initialized in a winter month (December) and in a summer month (July)
683 and runs free from this point to about 3-4 months, covering a dry and a wet period,
684 respectively. It may be concluded that in both cases, positive differences are present until the
685 end of the simulations. The largest deviations are found during dry periods in both scenarios.



686 Soil is more sensitive to initialization during dry periods, i.e., longer spin-up times (time the
687 soil needs to restore quasi-equilibrium) are needed. RMSD is in both periods closer to zero
688 after heavy precipitation events. The upper level soil moisture rapidly reacts to precipitation,
689 soil conditions close to saturation result in the loss of soil moisture memory in the upper soil
690 level. The long-term impact of the initial dry or wet scenario, acts in a stochastic way after
691 heavy precipitation events, independently from the sign of the initial perturbation. Good
692 agreement was reached when comparisons between point-like and 10x10 km² simulations
693 with SURFEX-SAFRAN initialized with SMOS-L4^{3.0} data and in-situ soil moisture
694 measurements were made ($R^2 \sim 0.9$ and $\text{RMSD} < 0.04 \text{ m}^3/\text{m}^3$).

695 In this study, the comparison and suitability of different operational satellite products from the
696 SMOS platform is investigated to provide realistic information on the water content of the
697 soil. The comparison carried out helps drawing guidelines on best practices for the sensible
698 use of these products. Currently, there is not a consensus about what is the “best” SMOS
699 product. Different users utilize different products depending on their application rather than
700 based on performance arguments. This study and the conclusions obtained on the comparison
701 are important to provide information on the advantages and drawbacks of these datasets. The
702 high temporal and spatial resolution soil moisture maps obtained in this study could be of use
703 to build climatologies of SSM, as initial condition for convective system modelling, for flood
704 forecasting and for downstream local applications such as crop monitoring and crop
705 development strategies. Additionally, an accurate representation of SSM will permit the
706 calculation of SM profiles by application of e.g. exponential filters, which has been
707 demonstrated to be a successful technique. This is however, out of the scope of the paper, and
708 will be investigated in a follow-up research activity. Furthermore, the added value of the
709 SMOS-L4^{3.0}-1 km disaggregated product for initialization purposes is demonstrated, which
710 suggests its potential for assimilation purposes. Nevertheless, important aspects of the SMOS-



711 L4^{3.0} SSM product have still to be improved, namely its temporal availability (e.g. successful
712 investigations on the increase of SMOS-L3 temporal resolution to 3h are available (Louvet et
713 al. 2015)), its spatio-temporal correlation with in situ measurements over complex
714 topographic areas, in areas/periods with low spatial variability and in rainy periods when an
715 under-representation and rapid decay of SSM has been identified.

716

717

718

719

720

721

722

723

724

725

726

727

728

729

730



731 **Acknowledgements**

732 The authors acknowledge AEMET for supplying the precipitation data and the HyMeX
733 database teams (ESPRI/IPSL and SEDOO/Observatoire Midi-Pyrénées) for their help in
734 accessing the data. The SMOS products were obtained from CATDS (Centre Aval de
735 Traitement des Données SMOS) and SMOS-BEC (Barcelona Expert Center. We
736 acknowledge the support of the SURFEX-web team members. The ECMWF data was
737 obtained from <http://www.ecmwf.int>. Special thanks go to Pere Quintana for providing the
738 SAFRAN atmospheric forcing data. A. Coll's work was supported by both National Spanish
739 Space Research Programme projects MIDAS-6 (MIDAS-6/UVEG. SMOS Ocean Salinity and
740 Soil Moisture Products. Improvements and Applications Demonstration) and MIDAS-7
741 (MIDAS-7/UVEG. SMOS and Future Missions Advanced Products and Applications). The
742 first author's research is supported by the Bundesministerium für Bildung und Forschung
743 (BMBF; German Federal Ministry of Education and Research).

744

745

746

747

748

749

750

751



752 **References**

753 ARRAY Systems Computing Inc., CESBIO, IPSL-Service d'Aéronomie, INRA-EPHYSE,
754 Reading University, Tor Vergata University. Algorithm Theoretical Basis Document (ATBD)
755 for the SMOS Level 2 Soil Moisture Processor Development Continuation Project. ESA No.:
756 SO-TN-ARR-L2PP-0037 Issue: 3.9 Array No.: ASC_SMPPD_037 Date: October 24, 2014

757

758 Bircher, S., Skou, N., Jensen, K. H., Walker, J. P., & Rasmussen, L. (2012). A soil moisture
759 and temperature network for SMOS validation in Western Denmark. *Hydrology and Earth*
760 *System Sciences*, 16(5), 1445-1463.

761

762 Bolle, H.-J., Eckardt, M., Koslowsky, D., Maselli, F., Meliá Miralles, J., Menenti, M., Olesen,
763 F.-S., Petkov, L., Rasool, I., Van de Griend, A.A. (Editors). Contributing Authors: H. Billing,
764 A. Gitelson, F. Götsche, A. Jochum-Osann, E. Lopez-Baeza, F. Meneguzzo, J. Moreno, F.
765 Nerry, P. Rossini, F. Veroustraete, R. Vogt, P.J. Van Oeleven. *Mediterranean Landsurface*
766 *Processes Assessed From Space. Chapter 6 From Research to Application. Regional Climate*
767 *Studies Series*. Springer-Verlag Berlin Heidelberg, ISBN: 978-3-540-40151-3 (Print) 978-3-
768 540-45310-9 (Online) (2006)

769

770 Boone, A., Calvet, J.-C., & Noilhan, J. (1999). Inclusion of a Third Soil Layer in a Land
771 Surface Scheme Using the Force-Restore Method. *Journal of Applied Meteorology*, 38,
772 1611–1630. [https://doi.org/10.1175/1520-0450\(1999\)038<1611:IOATSL>2.0.CO;2](https://doi.org/10.1175/1520-0450(1999)038<1611:IOATSL>2.0.CO;2)



- 773 Bosch, D. D., J. M. Sheridan, and L. K. Marshall (2007), Precipitation, soil moisture, and
774 climate database, Little River Experimental Watershed, Georgia, United States, Water Resour.
775 Res., 43, W09472, doi:10.1029/2006WR005834
776
- 777 Brocca, L., Melone, F., Moramarco, T., Wagner, W., & Hasenauer, S. (2010). ASCAT soil
778 wetness index validation through in situ and modeled soil moisture data in central Italy.
779 Remote Sensing of Environment, 114(11), 2745-2755.
780
- 781 Calvet, J.-C., Noilhan, J., & Bessemoulin, P. (1998). Retrieving the Root-Zone Soil Moisture
782 from Surface Soil Moisture or Temperature Estimates: A Feasibility Study Based on Field
783 Measurements. Journal of Applied Meteorology, 37(1995), 371–386.
784 [https://doi.org/10.1175/1520-0450\(1998\)037<0371:RTRZSM>2.0.CO;2](https://doi.org/10.1175/1520-0450(1998)037<0371:RTRZSM>2.0.CO;2)
785
- 786 | Clapp, R. B., & Hornberger, G. M. (1978). Empirical equations for some soil hydraulic
787 properties. Water resources research, 14(4), 601-604.
788
- 789 Cosby, B. J., Hornberger, G. M., Clapp, R. B., & Ginn, T. (1984). A statistical exploration of
790 the relationships of soil moisture characteristics to the physical properties of soils. Water
791 resources research, 20(6), 682-690.
792



793 Cosh, M. H., Jackson, T. J., Bindlish, R., & Prueger, J. H. (2004). Watershed scale temporal
794 and spatial stability of soil moisture and its role in validating satellite estimates. Remote
795 sensing of Environment, 92(4), 427-435.

796

797 De Lannoy, G. J., & Reichle, R. H. (2016). Global assimilation of multiangle and
798 multipolarization SMOS brightness temperature observations into the GEOS-5 catchment
799 land surface model for soil moisture estimation. Journal of Hydrometeorology, 17(2), 669-
800 691.

801

802 Delwart, S., Bouzinac, C., Wursteisen, P., Berger, M., Drinkwater, M., Martín-Neira, M., &
803 Kerr, Y. H. (2008). SMOS validation and the COSMOS campaigns. IEEE Transactions on
804 Geoscience and Remote Sensing, 46(3), 695-704.

805

806 Dente, L., Su, Z., & Wen, J. (2012). Validation of SMOS soil moisture products over the
807 Maqu and Twente regions. Sensors, 12(8), 9965-9986.

808

809 Drobinski P., V. Ducrocq, P. Alpert, E. Anagnostou, K. Béranger, M. Borga, I. Braud, A.
810 Chanzy, S. Davolio, G. Delrieu, C. Estournel, N. Filali Boubrahmi, J. Font, V. Grubišić, S.
811 Gualdi, V. Homar, B. Ivančan-Picek, C. Kottmeier, V. Kotroni, K. Lagouvardos, P. Lionello,
812 M. C. Llasat, W. Ludwig, C. Lutoff, A. Mariotti, E. Richard, R. Romero, R. Rotunno, O.
813 Roussot, I. Ruin, S. Somot, I. Taupier-Letage, J. Tintore, R. Uijlenhoet, and H. Wernli, 2014.
814 HyMeX: A 10-year multidisciplinary program on the Mediterranean water cycle. Bull. Amer.
815 Meteor. Soc., 95, 1063–1082. doi: <http://dx.doi.org/10.1175/BAMS-D-12-00242.1>



816

817 Ducrocq Véronique, Isabelle Braud, Silvio Davolio, Rossella Ferretti, Cyrille Flamant,
818 Agustin Jansa, Norbert Kalthoff, Evelyne Richard, Isabelle Taupier-Letage, Pierre-Alain
819 Ayral, Sophie Belamari, Alexis Berne, Marco Borga, Brice Boudevillain, Olivier Bock, Jean-
820 Luc Boichard, Marie-Noëlle Bouin, Olivier Bousquet, Christophe Bouvier, Jacopo Chiggiato,
821 Domenico Cimini, Ulrich Corsmeier, Laurent Coppola, Philippe Cocquerez, Eric Defer,
822 Julien Delanoë, Paolo Di Girolamo, Alexis Doerenbecher, Philippe Drobinski, Yann
823 Dufournet, Nadia Fourrié, Jonathan J. Gourley, Laurent Labatut, Dominique Lambert, Jérôme
824 Le Coz, Frank S. Marzano, Gilles Molinié, Andrea Montani, Guillaume Nord, Mathieu Nuret,
825 Karim Ramage, William Rison, Odile Roussot, Frédérique Said, Alfons Schwarzenboeck,
826 Pierre Testor, Joël Van Baelen, Béatrice Vincendon, Montserrat Aran, and Jorge Tamayo,
827 2014. HyMeX-SOP1: The field campaign dedicated to heavy precipitation and flash flooding
828 in the Northwestern Mediterranean. *Bull. Amer. Meteor. Soc.*, 95, 1083–1100. doi:
829 <http://dx.doi.org/10.1175/BAMS-D-12-00244.1>

830

831 Duffourg, F., & Ducrocq, V. (2011). Origin of the moisture feeding the Heavy Precipitating
832 Systems over Southeastern France. *Natural Hazards and Earth System Sciences*, 11(4), 1163.

833

834 Duffourg, F., & Ducrocq, V. (2013). Assessment of the water supply to Mediterranean heavy
835 precipitation: a method based on finely designed water budgets. *Atmospheric Science Letters*,
836 14(3), 133-138.

837



838 Durand, Y., E. Brun, L. Mérindol, G. Guyomarc'h, B. Lesaffre, E. Martin, A meteorological
839 estimation of relevant parameters for snow models, *Ann. Glaciol.* 18 (1993) 65–71.

840

841 Durand, Y., G. Giraud, M. Laternser, P. Etchevers, L. Mérindol, B. Lesaffre, Reanalysis of 47
842 Years of Climate in the French Alps (1958–2005): Climatology and Trends for Snow Cover,
843 *J. Appl. Meteorol. Climatol.* 48 (2009) 2487–2512.

844

845 Entekhabi, D., Rodriguez-Iturbe, I., & Castelli, F. (1996). Mutual interaction of soil moisture
846 state and atmospheric processes. *Journal of Hydrology*, 184(1-2), 3-17.

847

848 FAO; World reference base for soil resources 2014 international soil classification system for
849 naming soils and creating legends for soil maps. Rome: FAO, 2014.

850

851 Gherboudj, I., Magagi, R., Goïta, K., Berg, A. A., Toth, B., & Walker, A. (2012). Validation
852 of SMOS data over agricultural and boreal forest areas in Canada. *IEEE Transactions on*
853 *Geoscience and Remote Sensing*, 50(5), 1623-1635.

854

855 GTOPO30 Documentation, U.S. Geological Survey, 1996, Global 30 Arc-Second Elevation

856 A. Gonzalez-Zamora, N. Sánchez, J. Martinez-Fernandez, A. Gumuzzio, M. Piles, E.
857 Olmedo. Long-Term SMOS Soil Moisture Products: A Comprehensive Evaluation across



858 Scales and Methods in the Duero Basin Physics and Chemistry of the Earth, Parts A/B/C, 83–
859 84 (2015), pp. 123–136 <http://dx.doi.org/10.1016/j.pce.2015.05.009>

860

861 Hirschi, M., Seneviratne, S. I., Alexandrov, V., Boberg, F., Boroneant, C., Christensen, O. B.,
862 and Stepanek, P. (2011). Observational evidence for soil-moisture impact on hot extremes in
863 southeastern Europe. *Nature Geoscience*, 4(1), 17.

864

865 Jansa, J., Erb, A., Oberholzer, H. R., Šmilauer, P., & Egli, S. (2014). Soil and geography are
866 more important determinants of indigenous arbuscular mycorrhizal communities than
867 management practices in Swiss agricultural soils. *Molecular ecology*, 23(8), 2118–2135.

868

869 Jones, M. O., L. A. Jones, J. S. Kimball, and K. C. McDonald (2011), Satellite passive
870 microwave remote sensing for monitoring global land surface phenology, *Remote Sens.*
871 *Environ.*, 115(4), 1102–1114, doi:10.1016/j.rse.2010.12.015.

872

873 Juglea, S., Kerr, Y., Mialon, A., Lopez-Baeza, E., Braithwaite, D., & Hsu, K. (2010). Soil
874 moisture modelling of a SMOS pixel: Interest of using the PERSIANN database over the
875 Valencia Anchor Station. *Hydrology and Earth System Sciences*, 14(8), 1509–1525.
876 <https://doi.org/10.5194/hess-14-1509-2010>

877

878 Juglea, S., Kerr, Y., Mialon, A., Wigneron, J. P., Lopez-Baeza, E., Cano, A., ... Delwart, S.
879 (2010). Modelling soil moisture at SMOS scale by use of a SVAT model over the Valencia



880 Anchor Station. Hydrology and Earth System Sciences, 14(5), 831–846.

881 <https://doi.org/10.5194/hess-14-831-2010>

882

883 Kerr, Y. H. (2007). Soil moisture from space: Where are we?. Hydrogeology journal, 15(1),

884 117-120.

885

886 Kerr, Y. H., Waldteufel, P., Wigneron, J. P., Delwart, S., Cabot, F., Boutin, J., ... & Juglea, S.

887 E. (2010). The SMOS mission: New tool for monitoring key elements of the global water

888 cycle. Proceedings of the IEEE, 98(5), 666-687.

889

890 Kerr, Y. H., Waldteufel, P., Wigneron, J. P., Martinuzzi, J. A. M. J., Font, J., & Berger, M.

891 (2001). Soil moisture retrieval from space: The Soil Moisture and Ocean Salinity (SMOS)

892 mission. IEEE transactions on Geoscience and remote sensing, 39(8), 1729-1735.

893

894 Khodayar, S., Raff, F., Kalthoff, N. 2015. Diagnostic Study of a High Precipitation Event in

895 the Western Mediterranean Region: Adequacy of Current operational Networks

896 Quart. J. Roy. Meteor. Soc. DOI: 10.1002/qj.2600

897

898 Khodayar, S., Sehlinger, A., Feldmann, H., & Kottmeier, C. (2015). Sensitivity of soil

899 moisture initialization for decadal predictions under different regional climatic conditions in

900 Europe. International Journal of Climatology, 35(8), 1899-1915.

901



902 Koster, R. D., Dirmeyer, P. A., Guo, Z., Bonan, G., Chan, E., Cox, P., ... & Liu, P. (2004).
903 Regions of strong coupling between soil moisture and precipitation. *Science*, 305(5687),
904 1138-1140.

905

906 Le Moigne, P., Boone, A., Calvet, J. C., Decharme, B., Faroux, S., Gibelin, A. L., ... &
907 Mironov, D. (2009). SURFEX scientific documentation. Note de centre (CNRM/GMME),
908 Météo-France, Toulouse, France.

909

910 Masson, V., Champeaux, J. L., Chauvin, F., Meriguet, C., & Lacaze, R. (2003). A global
911 database of land surface parameters at 1-km resolution in meteorological and climate models.
912 *Journal of Climate*, 16(9), 1261–1282. <https://doi.org/10.1175/1520-0442-16.9.1261>

913

914 Merlin, O., Rüdiger, C., Al Bitar, A., Richaume, P., Walker, J. P., & Kerr, Y. H. (2012).
915 Disaggregation of SMOS soil moisture in Southeastern Australia. *IEEE Transactions on*
916 *Geoscience and Remote Sensing*, 50(5), 1556–1571. [http://dx.doi.org/10.1109/TGRS.](http://dx.doi.org/10.1109/TGRS.2011.2175000)
917 2011.2175000.

918

919 Noilhan, J., & Planton, S. (1989). A Simple Parameterization of Land Surface Processes for
920 Meteorological Models. *Monthly Weather Review*. [https://doi.org/10.1175/1520-](https://doi.org/10.1175/1520-0493(1989)117<0536:ASPOLS>2.0.CO;2)
921 0493(1989)117<0536:ASPOLS>2.0.CO;2

922

923 | Piles, M., Camps, A., Vall-Llossera, M., Corbella, I., Panciera, R., Rudiger, C., ... Walker, J.



- 924 (2011). Downscaling SMOS-derived soil moisture using MODIS visible/infrared data. IEEE
925 Transactions on Geoscience and Remote Sensing, 49(9), 3156–3166.
926 <https://doi.org/10.1109/TGRS.2011.2120615>
927
- 928 Piles, M., Sánchez, N., Vall-Llossera, M., Camps, A., Martínez-Fernandez, J., Martinez, J., &
929 Gonzalez-Gambau, V. (2014). A downscaling approach for SMOS land observations:
930 Evaluation of high-resolution soil moisture maps over the Iberian peninsula. IEEE Journal of
931 Selected Topics in Applied Earth Observations and Remote Sensing, 7(9), 3845–3857.
932 <https://doi.org/10.1109/JSTARS.2014.2325398>
933
- 934 Piles, M., Vall-Llossera, M., Camps, A., Sanchez, N., Martinez-Fernandez, J., Martinez, J., ...
935 Riera, R. (2013). On the synergy of SMOS and Terra/Aqua MODIS: High resolution soil
936 moisture maps in near real-time. International Geoscience and Remote Sensing Symposium
937 (IGARSS), 3423–3426. <https://doi.org/10.1109/IGARSS.2013.6723564>
938
- 939 Quintana-Segui, P., Le Moigne, P., Durand, Y., Martin, E., Habets, F., Baillon, M., ... &
940 Morel, S. (2008). Analysis of near-surface atmospheric variables: Validation of the SAFRAN
941 analysis over France. Journal of applied meteorology and climatology, 47(1), 92-107.
942
- 943 Quintana-Seguí, P., Peral, C., Turco, M., Llasat, M. C., & Martin, E. (2016). Meteorological
944 Analysis Systems in North-East Spain: Validation of SAFRAN and SPAN. Journal of
945 Environmental Informatics, 27(2).



946

947 Raveh-Rubin, S., and Wernli, H. (2015). Large-scale wind and precipitation extremes in the
948 Mediterranean: a climatological analysis for 1979–2012. *Quarterly Journal of the Royal*
949 *Meteorological Society*, 141(691), 2404-2417.

950

951 Robock, A., Vinnikov, K. Y., Srinivasan, G., Entin, J. K., Hollinger, S. E., Speranskaya, N.
952 A., ... & Namkhai, A. (2000). The global soil moisture data bank. *Bulletin of the American*
953 *Meteorological Society*, 81(6), 1281-1299.

954

955 Rosenbaum, U., H. R. Bogen, M. Herbst, J. A. Huisman, T. J. Peterson, A. Weuthen, A. W.
956 Western, and H. Vereecken (2012), Seasonal and event dynamics of spatial soil moisture
957 patterns at the small catchment scale, *WaterResour.Res.*, 48, W10544,
958 doi:10.1029/2011WR011518.

959

960 Sanchez N., J. Martinez-Fernandez, A. Scaini and C. Perez-Gutierrez, "Validation of the
961 SMOS L2 Soil Moisture Data in the REMEDHUS Network (Spain)," in *IEEE Transactions*
962 *on Geoscience and Remote Sensing*, vol. 50, no. 5, pp. 1602-1611, May 2012. doi:
963 10.1109/TGRS.2012.2186971

964

965 Sánchez-Ruiz, S., Piles, M., Sánchez, N., Martínez-Fernández, J., Vall-llossera, M., &
966 Camps, A. (2014). Combining SMOS with visible and near/shortwave/thermal infrared
967 satellite data for high resolution soil moisture estimates. *Journal of Hydrology*, 516, 273–283.
968 <https://doi.org/10.1016/j.jhydrol.2013.12.047>



969

970 Schubert, M., & Boche, H. (2004). Solution of the multiuser downlink beamforming problem
971 with individual SINR constraints. *IEEE Transactions on Vehicular Technology*, 53(1), 18-28.

972

973 Schwank, M., Wigneron, J. P., Lopez-Baeza, E., Volksch, I., Matzler, C., & Kerr, Y. H.
974 (2012). L-band radiative properties of vine vegetation at the MELBEX III SMOS cal/val site.
975 *IEEE Transactions on Geoscience and Remote Sensing*, 50(5), 1587-1601.

976

977 Seneviratne, S. I., Corti, T., Davin, E. L., Hirschi, M., Jaeger, E. B., Lehner, I., ... & Teuling,
978 A. J. (2010). Investigating soil moisture–climate interactions in a changing climate: A review.
979 *Earth-Science Reviews*, 99(3), 125-161.

980

981 Taylor, C. M., & Lebel, T. (1998). Observational evidence of persistent convective-scale
982 rainfall patterns. *Monthly Weather Review*, 126(6), 1597-1607.

983

984 Vautard, R., Yiou, P., D'andrea, F., De Noblet, N., Viovy, N., Cassou, C., ... & Fan, Y.
985 (2007). Summertime European heat and drought waves induced by wintertime Mediterranean
986 rainfall deficit. *Geophysical Research Letters*, 34(7).

987

988 J.-P. Vidal, E. Martin, L. Franchistéguy, M. Baillon, J.-M. Soubeyrou, A 50-year high-
989 resolution atmospheric reanalysis over France with the Safran system, *Int. J. Climatol.* 30
990 (2010) 1627–1644.



991

992 Walker, J., & Rowntree, P. R. (1977). The effect of soil moisture on circulation and rainfall in
993 a tropical model. *Quarterly Journal of the Royal Meteorological Society*, 103(435), 29-46.

994

995 Western, A. W., Grayson, R. B., & Blöschl, G. (2002). Scaling of soil moisture: A hydrologic
996 perspective. *Annual Review of Earth and Planetary Sciences*, 30(1), 149-180.

997

998 Wigneron, J. P., Calvet, J. C., Pellarin, T., Van de Griend, A. A., Berger, M., & Ferrazzoli, P.
999 (2003). Retrieving near-surface soil moisture from microwave radiometric observations:
1000 current status and future plans. *Remote Sensing of Environment*, 85(4), 489-506.

1001

1002 Wigneron, J.-P., M. Schwank, E. Lopez Baeza, Y. Kerr, N. Novello, C. Millan, C. Moisy, P.
1003 Richaume, A. Mialon, A. Al Bitar, F. Cabot, H. Lawrence, D. Guyon, J-C Calvet, J. P. Grant,
1004 P. de Rosnay, A. Mahmoodi, S. Delwart, S. Mecklenburg (2012). First Evaluation of the
1005 Simultaneous SMOS and ELBARA-II Observations in the Mediterranean Region. *Remote*
1006 *Sensing of Environment*, 124, 26–37

1007

1008 Zampieri, M., F. D'Andrea, R. Vautard, P. Ciais, N. de Noblet-Ducoudré, and P. Yiou, 2009:
1009 Hot European Summers and the Role of Soil Moisture in the Propagation of Mediterranean
1010 Drought. *J. Climate*, 22, 4747–4758, <https://doi.org/10.1175/2009JCLI2568.1>

1011

1012









1013

1014

1015 **Tables**

1016

1017 **Table 1:** Characteristics of soil moisture stations within the VAS domain.

NAME	STATION	DOMINANT VEGETATION USED FOR SIMULATIONS	TYPE OF VEGETATION	SAND	SILT	CLAY	ALTITUDE (m)	ANNUAL MEAN TEMPERATURE (°C)	ANNUAL MEAN PRECIPITATION (mm)
Melbex_I		Schrub	Schrub	0,47	0,38	0,15	849	(12-14)	451
Nicolas		Vineyard	Schrub/ Vineyard	0,47	0,35	0,18	859		
La Cubera		Vineyard	Vineyard	0,45	0,35	0,20	762		
Ezpeleta		Olive tree	Olive tree	0,44	0,39	0,17	781		
VAS		Vineyard	Vineyard	0,46	0,37	0,17	804		
Melbex_II		Vineyard	Vine stump/ Vine row	0,45	0,29	0,26	797		

1018

1019

1020

1021

1022

1023

1024

1025

1026

1027

1028

1029

1030

1031



1032

1033

1034

1035 **Table 2:** Number of days (percentage) in which the SMOS (ascendant and descendent
1036 swaths) coverage is higher than 50 %.

1037

LEVEL SMOS	SEPTEMBER		OCTOBER		NOVEMBER		SON	
	days	%	days	%	days	%	days	%
L4 ^{2.0} (~1km)	10	34	9	31	9	31	28	32
L4 ^{3.0} (~1km)	23	74	29	90	30	100	82	92
L2 (~15km)	20	67	28	90	28	93	76	83
L3 (~25km)	22	73	29	93	29	96	80	88

1038

1039

1040

1041

1042

1043

1044

1045

1046

1047

1048

1049

1050

1051

1052

1053

1054

1055



1056

1057

1058 **Table 3:** Statistics of daily areal averages of SMOS-L2 and SMOS-L4^{3.0} soil moisture versus
1059 ground-based soil moisture measurements over OBS. SMOS descendent orbits are selected
1060 for the comparison.

1061

OBS vs SMOS-L2	Slope	R2	Bias	CRMS	OBS vs SMOS-L4 ^{3.0}	Slope	R2	Bias	CRMS
DJF	1.1	0.5	-0.09	0.03	DJF	1.0	0.7	-0.03	0.04
MAM	0.6	0.2	-0.07	0.03	MAM	0.6	0.4	-0.03	0.03
JJA	0.3	0.01	-0.02	0.03	JJA	0.1	0.01	-0.003	0.03
SON	1.1	0.8	-0.02	0.04	SON	0.8	0.7	-0.003	0.04

1062

SMOSL2 vs SMOSL4 ^{3.0}	M-I	M-II	VAS	NIC	EZ	LC	OBS (mean all stations)
DJF							
Slope	0.17/-0.04	1.0/1.7	1.6/2.3	1.1/1.7	0.8/0.9	0.9/1.7	1.1/0.6
R2	0.02/0.01	0.6/0.5	0.8/0.5	0.9/0.7	0.5/0.2	0.7/0.7	0.5/0.7
MB	-0.03/-0.08	-0.08/-0.14	0.01/-0.04	0.006/-0.05	0.03/-0.02	0.004/-0.05	-0.09/-0.03
CRMSD	0.04/0.03	0.03/0.02	0.04/0.03	0.03/0.03	0.04/0.03	0.04/0.03	0.03/0.04
MAM							
Slope	0.4/0.36	0.6/0.4	0.8/0.6	0.6/0.8	0.5/0.3	0.9/0.7	0.6/0.6
R2	0.2/0.08	0.3/0.04	0.5/0.15	0.9/0.5	0.3/0.14	0.4/0.2	0.2/0.4
MB	-0.04/-0.08	-0.08/-0.11	0.005/-0.03	0.003/-0.03	0.02/-0.02	-0.02/-0.05	-0.07/-0.03
CRMSD	0.03/0.03	0.03/0.03	0.03/0.03	0.03/0.03	0.04/0.03	0.03/0.03	0.03/0.03
JJA							
Slope	0.26/0.38	0.3/0.4	0.02/0.15	0.1/0.3	0.08/-0.04	0.05/0.06	0.3/0.1
R2	0.02/0.01	0.04/0.005	0.001/0.002	0.8/0.17	0.003/0.012	0.01/0.003	0.01/0.01
MB	-0.01/-0.03	-0.04/-0.05	0.03/0.012	0.01/0.002	0.05/0.04	0.03/0.02	-0.02/-0.003
CRMSD	0.03/0.03	0.03/0.03	0.03/0.03	0.03/0.03	0.03/0.03	0.03/0.03	0.03/0.03
SON							
Slope	0.69/1.06	0.9/1.3	1.2/1.7	0.8/1.2	0.7/1.1	0.8/1.3	1.1/0.8
R2	0.5/0.6	0.6/0.6	0.7/0.8	0.9/0.7	0.8/0.7	0.8/0.7	0.8/0.07
MB	-0.02/-0.04	-0.03/-0.05	0.04/-0.03	0.03/0.006	0.03/0.01	0.04/0.02	-0.02/-0.003
CRMSD	0.04/0.04	0.04/0.04	0.04/0.04	0.04/0.04	0.04/0.04	0.04/0.04	0.04/0.04

1063

1064

1065

1066

1067

1068

1069

1070

1071

1072

1073



1074

1075

1076 **Table 4:** Statistics of daily areal averages of ground-based SSM measurements in the OBS
1077 area versus point-like SURFEX-ISBA simulations at the same sites.

1078

	M-I	M-II	VAS	NIC	EZ	LC	OBS
All period							
Slope	0.9	1.3	0.9	0.7	1.0	0.9	1.0
R2	0.8	0.8	0.8	0.8	0.8	0.7	0.9
MB	0.004	-0.012	0.011	0.006	0.02	0.006	0.005
CRMSD	0.02	0.02	0.02	0.02	0.01	0.02	0.02
DJF							
Slope	0.2	1.3	0.8	1.2	1.2	1.1	1.1
R2	0.03	0.4	0.4	0.7	0.7	0.5	0.6
MB	0.01	-0.03	0.02	0.03	0.02	0.03	0.01
CRMSD	0.04	0.05	0.03	0.04	0.03	0.03	0.04
MAM							
Slope	0.8	1.0	1.0	0.7	0.8	0.7	0.9
R2	0.5	0.4	0.6	0.4	0.6	0.5	0.6
MB	0.002	-0.02	0	0.01	0.01	-0.02	-0.004
CRMSD	0.04	0.02	0.03	0.04	0.03	0.04	0.04
JJA							
Slope	0.4	0.8	1.6	3	1.6	2	1.5
R2	0.7	0.8	0.7	0.5	0.7	0.6	0.8
MB	0.004	0.01	0.01	-0.02	0.02	0.005	0.005
CRMSD	0.04	0.02	0.03	0.04	0.03	0.04	0.04
SON							
Slope	0.9	1.1	0.9	0.8	1.0	1.1	1.0
R2	0.8	0.8	0.8	0.9	0.9	0.8	0.9
MB	0.002	0	0.01	0	0.02	0.01	0.006
CRMSD	0.04	0.006	0.03	0.04	0.04	0.03	0.04

1079

1080

1081

1082

1083

1084

1085

1086

1087

1088

1089

1090

1091

1092

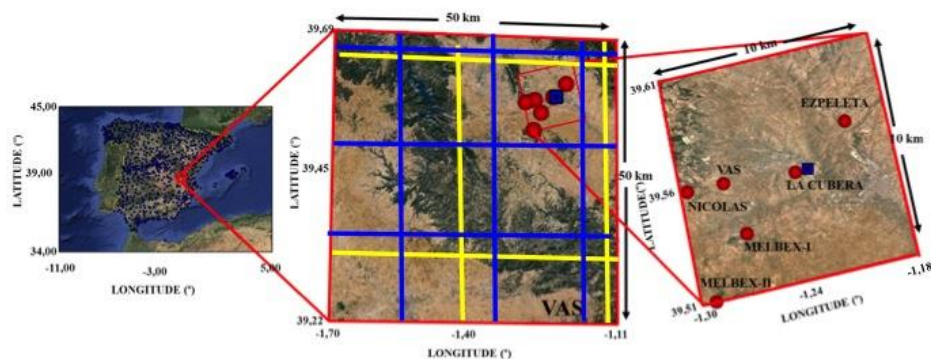


1093

1094

1095 **Figures**

1096



1097

1098

1099 **Figure 1:** Area of investigation and orography. Location of rain gauges from AEMET
1100 (Meteorological Service of Spain) is shown over the Iberian Peninsula (blue square dots).
1101 The positions of the soil moisture network stations within the 10x10 km² (OBS area) in the
1102 Valencia Anchor Station (VAS; 50x50 km²) area are indicated by red circles.

1103

1104

1105

1106

1107

1108

1109

1110

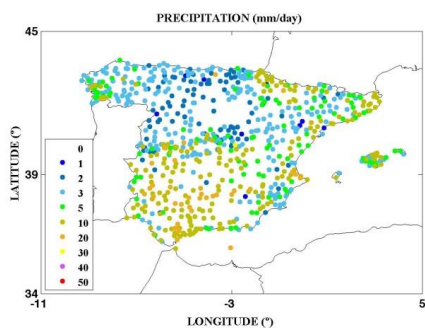
1111

1112

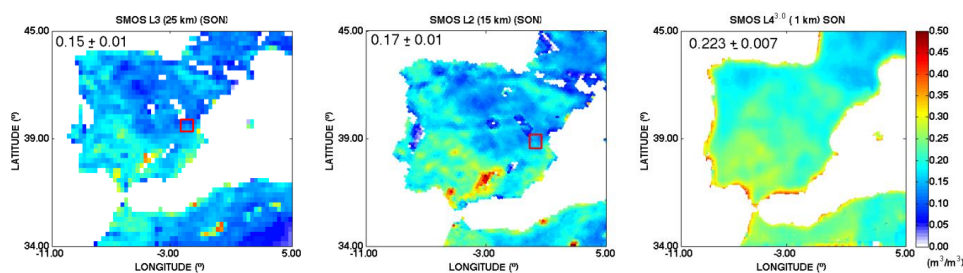


1113

1114



1115



1116

1117

1118 **Figure 2:** (a) Spatial distribution of precipitation over the Iberian Peninsula from the network
1119 of rain gauges of AEMET. The period of September to November (SON) 2012 is shown. (b)
1120 Spatial distribution of SMOS-derived soil moisture over the Iberian Peninsula (merged
1121 product: ascending and descending orbits, days with areal coverage higher than 50 % are
1122 considered).

1123

1124

1125

1126

1127

1128

1129

1130

1131

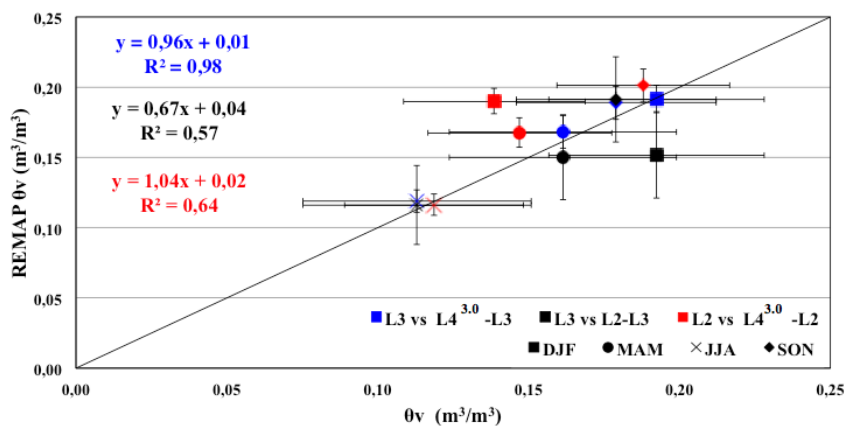
1132



1133

1134

1135



1136

1137

1138 **Figure 3:** SMOS-derived SSM products comparison from different operational levels over the
 1139 Iberian Peninsula.

1140

1141

1142

1143

1144

1145

1146

1147

1148

1149

1150

1151

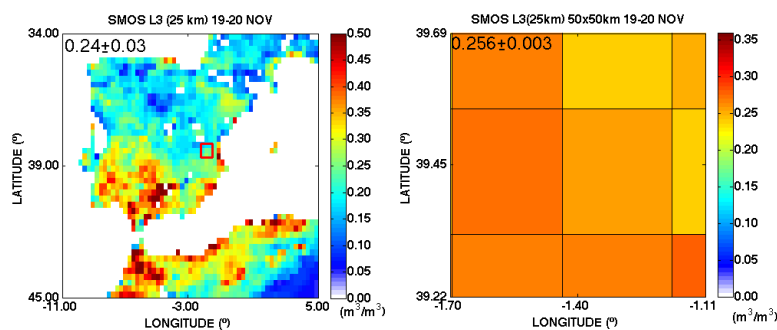
1152

1153

1154

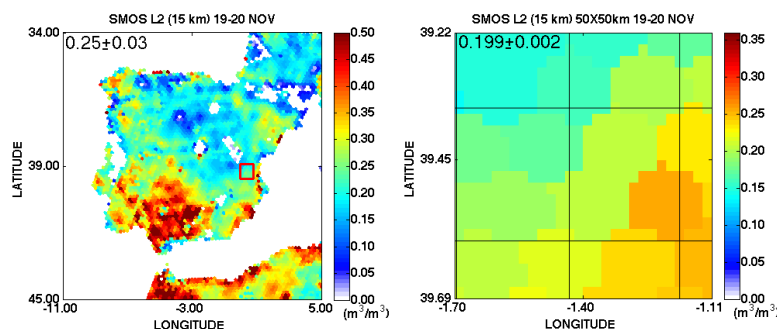


1155 (a)



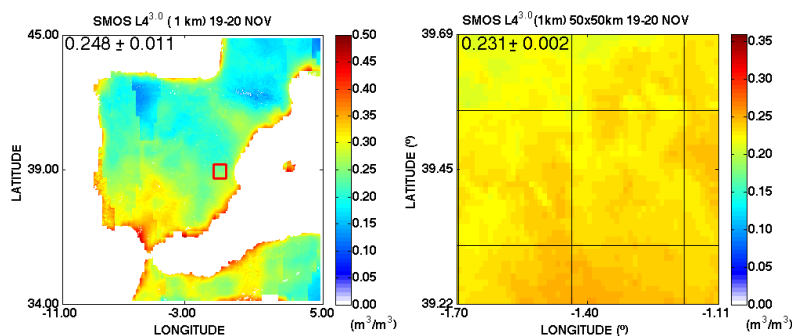
1156

1157 (b)



1158

1159 (c)



1160

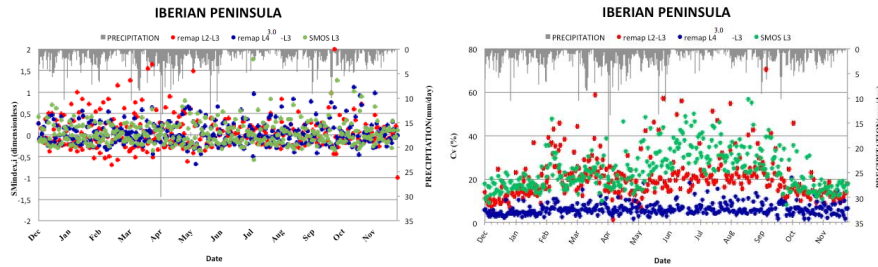
1161

1162 **Figure 4:** Spatial distribution of SMOS-derived soil moisture (merged product: ascending and
 1163 descending orbits are considered) over the Iberian Peninsula (left) and the VAS (right) as a
 1164 mean for the 19-20 November of 2012 (a) SMOS-L3 (~25 km), (b) SMOS-L2 (~15 km), (c)
 1165 SMOS-L4^{3.0} (~1 km). White empty pixels in (a) and (b) are indicative of a lack of data. Please
 1166 be aware of the different colour scale used for the IP and VAS.

1167



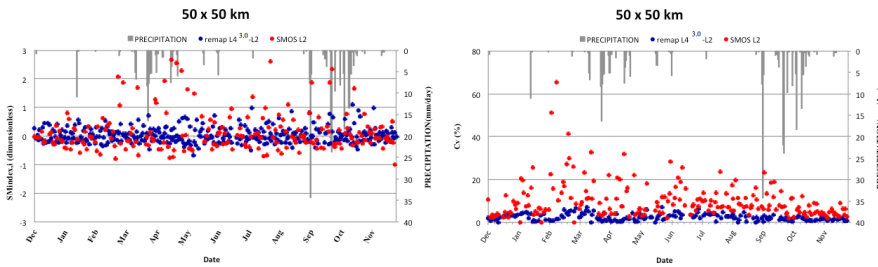
1168 (a)



1169

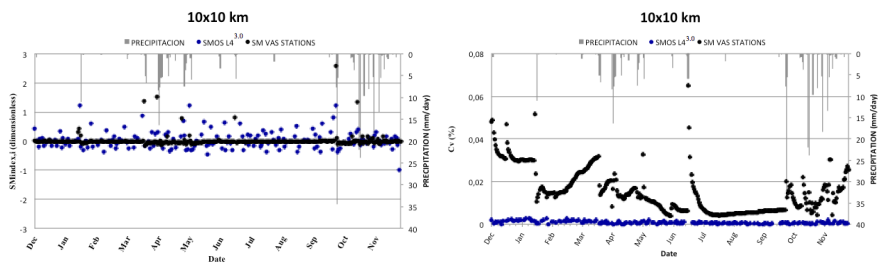
1170

1171 (b)



1172

1173 (c)



1174

1175 **Figure 5:** Averaged SMOS products and averaged ground-based observations of soil
 1176 moisture evolution over the Iberian Peninsula (IP; top), the VAS area (centre), and the OBS
 1177 area (bottom). Descending orbits are used. Precipitation from AEMET rain gauges on top.
 1178 Left) Soil moisture daily index ($\Theta_{v, index, i}$; dimensionless) and right) Coefficient of variation (Cv,
 1179 %).

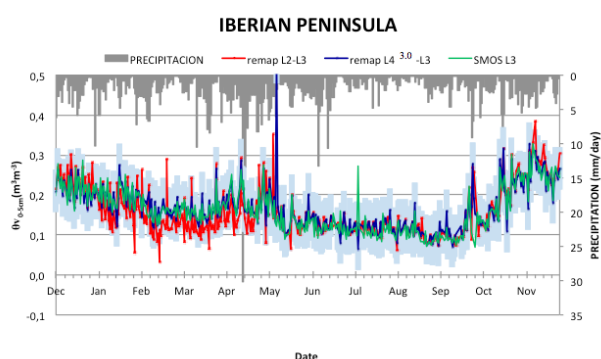
1180

1181

1182

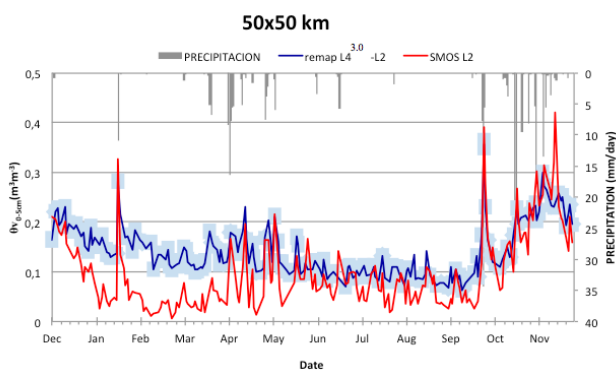


1183 (a)



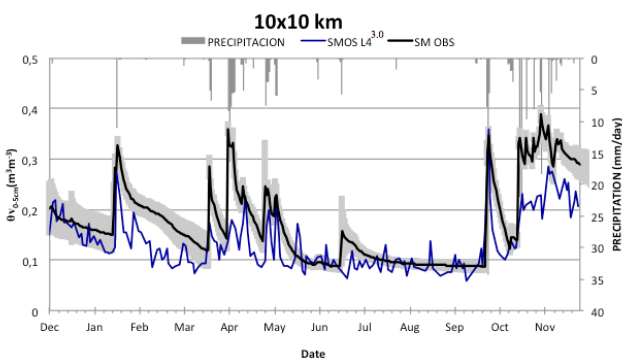
1184

1185 (b)



1186

1187 (c)

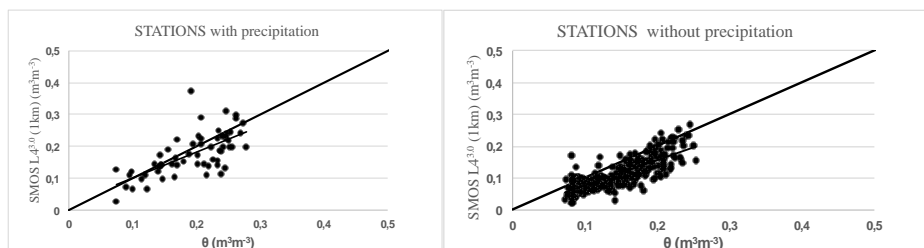


1188

1189 **Figure 6:** Temporal evolution of surface soil moisture time series averaged over the Iberian
1190 Peninsula (top), the VAS area (50 x 50 km²; centre) and the OBS area (10 x 10 km²; bottom).
1191 SMOS afternoon orbits are considered. Daily mean precipitation from the AEMET stations is
1192 shown on top of each plot. SMOS and remapped SMOS products are indicated in the plots.
1193 Shaded areas show standard deviations, respectively.



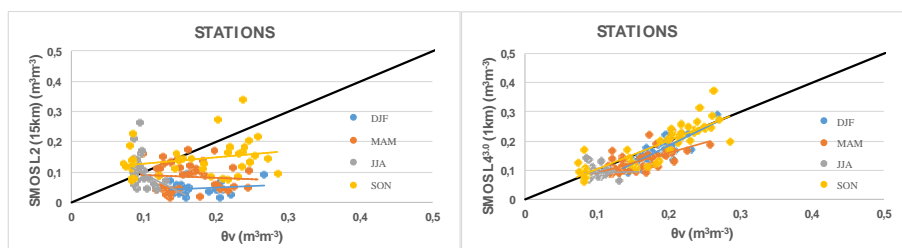
1194 (a)



1195

1196

1197 (b)

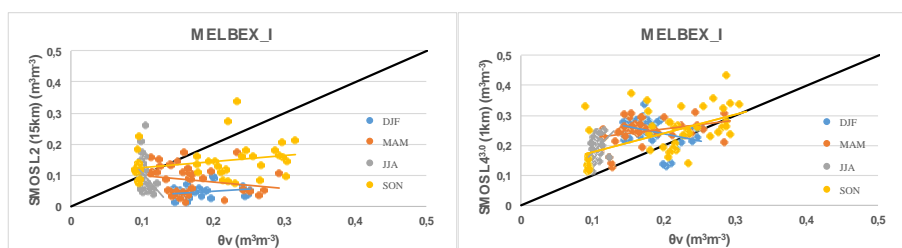


1198

1199

1200 (c)

1201



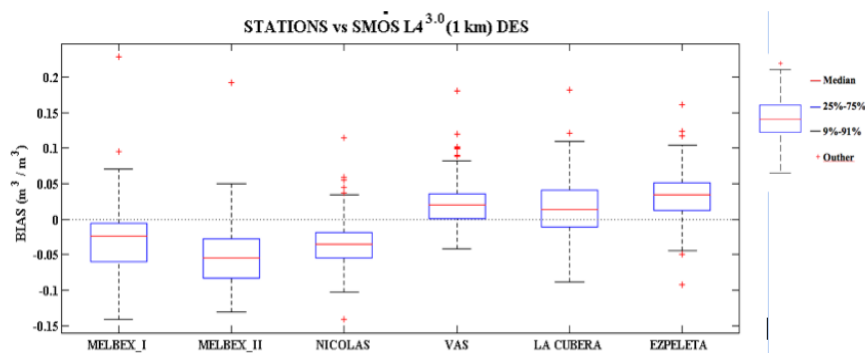
1202

1203

1204 **Figure 7:** Results of the seasonal analysis for the hydrological year starting in December
 1205 2011. Scatter plots of (a) SMOS-L4^{3.0} SSM (ascending and descending orbits) versus
 1206 averaged 10x10 km² in situ soil moisture measurements (left) for days with precipitation,
 1207 (right) and without precipitation (< 1 mm /d). (b) SMOS-L2 and SMOS-L4^{3.0} SSM (descending
 1208 orbits) versus averaged 10x10 km² in situ soil moisture measurements. (c) SMOS-L2 and
 1209 SMOS-L4^{3.0} SSM (descending orbits) versus point-like ground measurements from
 1210 MELBEX_I station, using the closest grid point. Segments are linear fit of seasonal data (3
 1211 months data). Statistics for individual comparisons at all stations are summarized in Table 3.



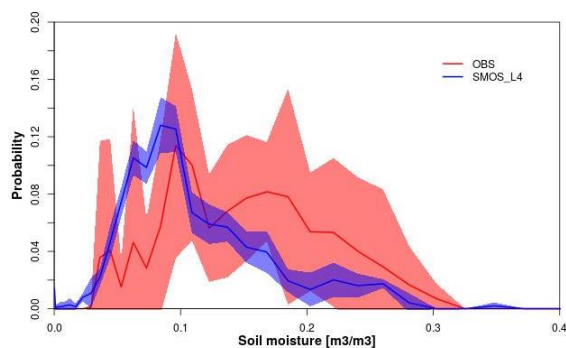
1212 (a)



1213

1214

1215 (b)



1216

1217 **Figure 8:** (a) Box plot of the comparison between point-like ground measurements at all
1218 stations over the VAS area and closest SMOS-L4^{3.0} SSM data. (b) Probability distribution
1219 function (PDF) of SSM from in situ observations and SMOS- L4^{3.0} SSM measurements. The
1220 standard deviations are indicated with shaded areas. Full lines represent the mean over all
1221 ground stations and over the 10 x 10 km² of the OBS area in VAS where the in SSM network
1222 is located.

1223

1224

1225

1226

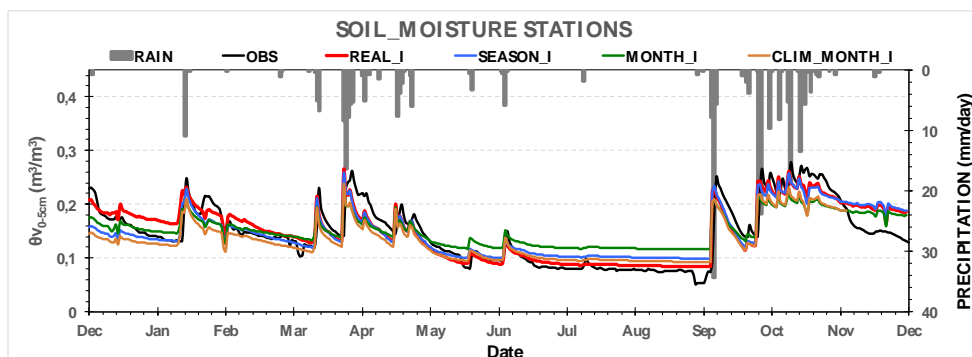
1227

1228



1229 (a)

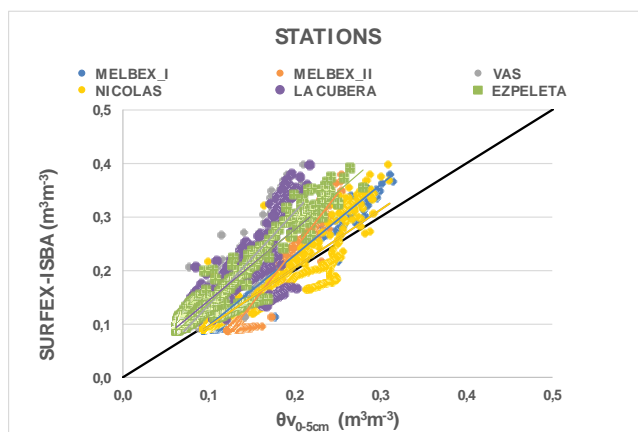
1230



1231

1232 (b)

1233



1234

1235

1236 **Figure 9:** (a) Temporal evolution of SSM in situ measurements and simulated SURFEX-
 1237 ISBA as a mean over all stations. All perturbation simulations are indicated. Precipitation
 1238 from AEMET stations is included at the top. (b) Scatter plot of temporal mean (over the whole
 1239 simulation period) SSM ground measurements versus SURFEX-ISBA simulations (realistic
 1240 initial scenario; REAL-I) at all stations. Statistics for all stations using the REAL-I initial
 1241 scenario are presented in Table 4.

1242

1243

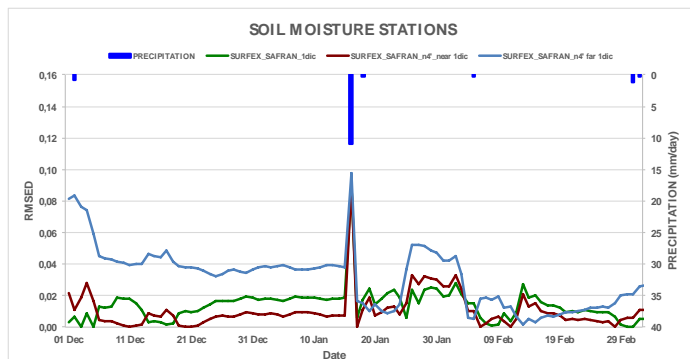
1244

1245

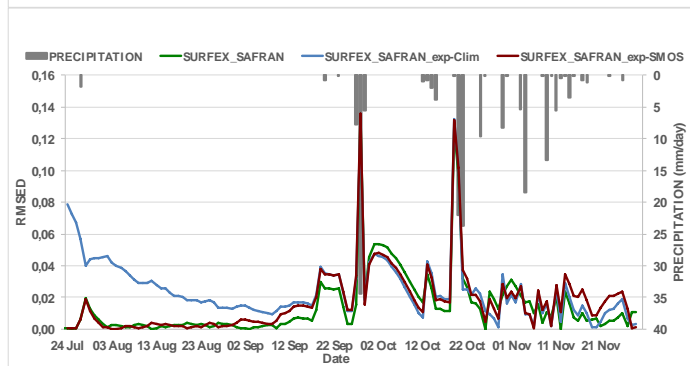


1246

1247 (a)



1248

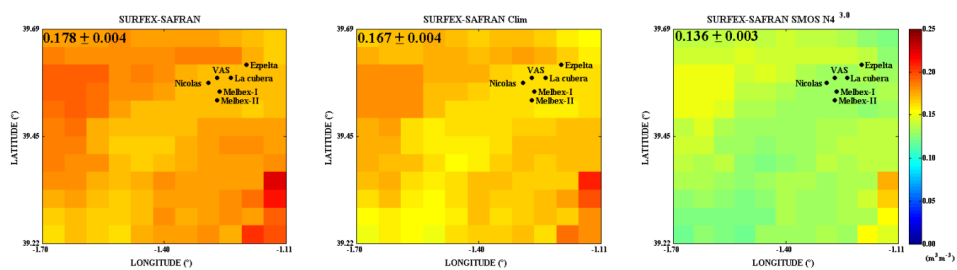


1249

1250

1251 (b)

1252



1253

1254

1255

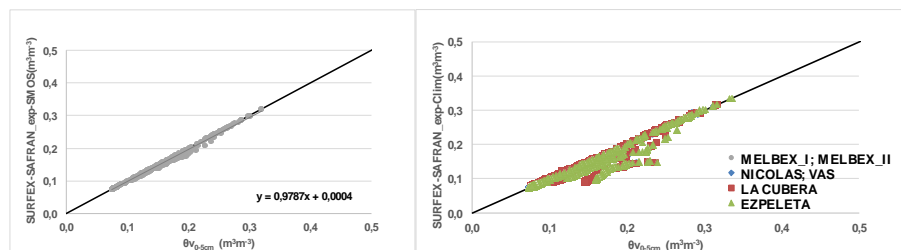
1256

1257



1258 (c)

1259



1260

1261

1262

1263 **Figure 10:** (a) RMSD for the daily mean SSM from the three SURFEX-ISBA simulations
1264 with perturbed initial SSM scenarios (details in section 4.3.2). (b) Spatial distribution of
1265 mean SSM for the winter simulation (a, left) for the 3 simulations. (c) Scatter plot depicting
1266 the comparison between in situ SSM observations and SURFEX-SAFRAN-SMOSL4^{3.0}
1267 simulations, as a mean over all stations (left) and for each of the stations (right).

1268

1269

1270

1271